Thesis, COLLÉGIALITÉ

Auteur : Hemmer, Marine
Promoteur(s) : Nokin, Marie-Julie
Faculté : Faculté de Médecine
Diplôme : Master en sciences biomédicales, à finalité approfondie
Année académique : 2023-2024
URI/URL : http://hdl.handle.net/2268.2/20513

Academic year 2023 – 2024
University of Liège
Laboratory of Developmental and Tumor Biology – GIGA Cancer

Evaluation of metabolic adaptations in $BRAF^{V600E}$ mutant melanoma cells treated with BRAF and MEK inhibitors

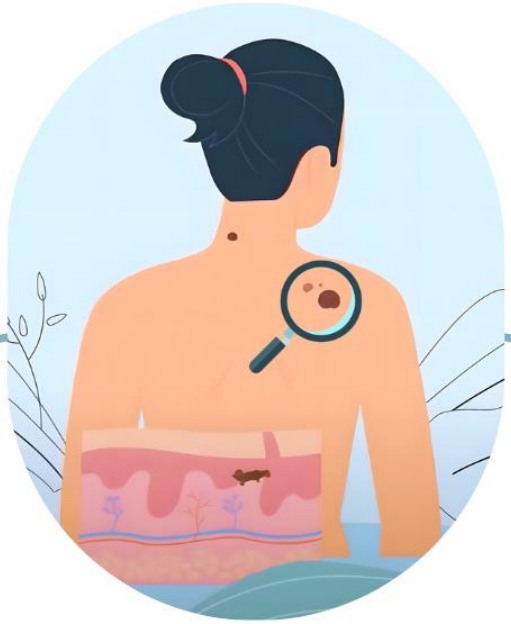

Master Thesis presented for the obtention of the Degree of Master in Biomedical Sciences

Marine HEMMER

Promoter: Dr Marie-Julie Nokin
Co-Promoter: Dr Rebekah Crake

Acknowledgements

First of all, I would like to extend my warmest thank to my primary supervisor, **Dr. Marie-Julie Nokin**, for welcoming me into her laboratory, and guiding me throughout this master's thesis project. Thank you for trusting me as your first “memory student”. Your guidance, precious advice and availability were crucial to the completion of this work.

I would also like to thank **Dr Rebekah Crake** for her patient and kind guidance, despite my sometimes broken English, throughout the realisation of this master thesis. You were always ready to listen and answer to all my questions. You taught me rigor and accuracy in my daily work in the laboratory. You were a precious help in my day-to-day learning and in the writing of this master thesis.

I also wish to thank **Laurine** for her help and support during this master thesis. Thank you for accompanying me in my learning and realization of FACS experiments and for being a fantastic person on whom I could count.

I would like to thank the whole LBTD team, and in particular the **+3 team**, for the wonderful welcome I received, where I was considered a full member of the laboratory and where I was able to benefit from a rich scientific environment to work in. Thank you for your encouragement and support throughout my internship. Our discussions, both scientific and personal, made this period very enjoyable. I am grateful to have joined a team like yours.

My thank to my buddies from the “**Cercle SBIM**”, Eva, Elisa, Chloé, Camille and Thomas for their support during this internship but also throughout these 5 years, I spent 5 years of learning but also of laughter and memories (moments at the Cercle, apéros, restaurants, trip to Athens) that will be engraved for life. Thank you for being such wonderful people, on whom I could count in moments of doubt and stress. A special mention to my **library buddies**, Chloé, Elisa and Nora, with whom I spent hours studying; our laughter and breaks in the sun brightened up those difficult times.

Finally, I would like to thank **my family** and **my friends** for their unconditional moral support and encouragement throughout the realisation of this master thesis, as well as over the past 5 years.

Marine alias *Pioupiou*

Abstract

The V600E mutation of the *BRAF* gene, involved in the MAP kinase pathway, is present in many cancers, including melanoma. Patients with this type of cancer are treated with targeted therapy combining Dabrafenib, acting specifically on the mutated form of BRAF, and Trametinib, targeting downstream MEK. Unfortunately, this approach rapidly leads to the development of acquired resistance. Persistent, treatment-tolerant cells are seen as the reservoir from which genetically resistant cells subsequently emerge, making tolerant cells a more effective therapeutic target than genetically resistant cells. Our hypothesis is that, by becoming persistent, cancer cells adapt their energetic metabolism and acquire potential therapeutically targetable vulnerabilities. The aim of this work is therefore to identify the energetic modifications developed by these persistent cells under the pressure of targeted therapy. Mitochondrial activity, quantity and localization were assessed using Seahorse flux analyzer, flow cytometry and confocal microscopy, respectively. Expression levels of various enzymes and transporters involved in glycolysis and mitochondrial activity were quantified using western blot and qPCR. Our results revealed increased mitochondrial activity in some persistent cells compared with their own parental cells. However, some discrepancies have been observed when deciphering further the expression levels of key metabolic players. Future investigations are required to better elucidate the metabolic adaptations of persister cells and identify specific targetable vulnerabilities.

Résumé

La mutation V600E du gène *BRAF*, impliqué dans la voie des MAP kinases, est présente dans de nombreux cancers y compris dans le mélanome. Les patients atteints par ces cancers sont traités par thérapie ciblée combinant le Dabrafenib, agissant spécifiquement sur la forme mutée de BRAF et le Trametinib ciblant MEK. Malheureusement, cette approche conduit rapidement au développement de résistance. Les cellules persistantes et tolérantes au traitement sont considérées comme le réservoir d'où émergent par la suite des cellules génétiquement résistantes, faisant de ces cellules tolérantes une cible thérapeutique plus intéressante que les cellules génétiquement résistantes. Notre hypothèse est, qu'en devenant persistantes, les cellules cancéreuses adaptent leur métabolisme énergétique et acquièrent des vulnérabilités potentiellement ciblables thérapeutiquement. Ce travail vise donc à identifier les modifications énergétiques développées par ces cellules persistantes sous la pression de la thérapie ciblée. L'activité, la quantité et la localisation des mitochondries ont été évaluées à l'aide d'un analyseur de flux Seahorse, de cytométrie en flux et de microscopie confocale, respectivement. Les niveaux d'expression de diverses enzymes et transporteurs impliqués dans la glycolyse et l'activité mitochondriale ont été quantifiés par Western blot et qPCR. Nos résultats ont révélé une activité mitochondriale accrue dans certaines cellules persistantes par rapport à leurs propres cellules parentales. Cependant, certaines divergences ont été observées lors de l'analyse plus approfondie des niveaux d'expression des principaux acteurs métaboliques. Des recherches futures sont nécessaires pour mieux élucider les adaptations métaboliques des cellules persistantes et identifier des vulnérabilités spécifiques ciblables thérapeutiquement.

Abbreviations

°C	Degree Celsius
ACLY	ATP Citrate Lyase
AS	Activation Segment
ATP	Adenosine Triphosphate
BRAFi	BRAF Inhibitor
BSA	Bovine Serum Albumin
cDNA	Complementary Deoxyribonucleic Acid
CLB	Complete Lysis Buffer
CR	Conserved Regions
Ct	Cycle threshold
D/T	Dabrafenib and Trametinib
DH	Drug Holiday
DMEM	Dulbecco's Modified Eagle Medium
DMSO	Dimethyl sulfoxide
DTEP	Drug-Tolerant Expanded Persister
DTP	Drug-tolerant Persister
EDTA	Ethylenediaminetetraacetic acid
EGF	Epidermal Growth Factor
EGFR	Epidermal Growth Factor Receptor
EMA	European Medicines Agency
ERK1	Extracellular-Signal-Regulated Protein Kinase 1
ERK2	Extracellular-Signal-Regulated Protein Kinase 2
ETC	Electron Transport Chain
FAO	Fatty Acid Oxidation
FBS	Fetal Bovine Serum
FCCP	Carbonyl cyanide-4 trifluoromethoxy phenylhydrazone
FDA	Food and Drug Administration
FGF	Fibroblast Growth Factor
FGR	Fibroblast Growth Factor Receptor

GDP	Guanosine Diphosphate
GFR	Growth Factor Receptor
GLUT1	Class 1 Glucose Transporter
Grb2	Growth Factor Binding Protein 2
GTP	Guanosine Triphosphate
HIF1α	Hypoxia-Inducible Factor 1α
HK2	Hexokinase 2
HMGCR	HMG-CoA reductase
IC50	Half Maximal Inhibitory Concentration
IDH1	Isocitrate Dehydrogenase 1
JNK	c-Jun N-terminal protein kinase
LDHA	Lactate dehydrogenase A
LHDA	Lactate dehydrogenase A
LUAD	Lung Adenocarcinoma
MAP	Mitogen-Activated Protein
MAPK	Mitogen-Activated Protein Kinase
MEK1	MAP and ERK kinase 1
MEK2	MAP and ERK kinase 2
MEKi	MEK inhibitor
MFI	Median Fluorescence Intensity
MIDs	Mass Isotopomere Distributions
Min	Minutes
MPC2	Mitochondrial Pyruvate Carrier 2
MTT	Thiazolyl Blue Tetrazolium Bromide
NSCLC	Non-Small Cell Lung Cancer
OCR	Oxygen Consumption Rate
ORR	Overall Response Rate
OS	Overall Survival
pACLY Ser455	Phosphorylated form of ACLY on serine in position 455
PBS	Phosphate-Buffered Saline
PDH	Pyruvate Dehydrogenase
PFS	Progression-free Survival

PGK1	Phosphoglycerate Kinase 1
pPDH Ser293	Phosphorylated form of PDH on serine in position 293
PTEN	Phosphatase and Tensin Homolog
PVDF	Polyvinylidene Fluoride
RAF	Rapidly Accelerated Fibrosarcoma
RAS	Rat Sarcoma Virus
RBD	RAS-Binding Domain
ROS	Reactive oxygen species
RPM	Rotations per minute
RTK	Receptor Tyrosine Kinase
RT-qPCR	Real Time Quantitative Polymerase Chain Reaction
SCLC	Small-Cell Lung Cancer
SDH	Succinate Dehydrogenase
SDHA	Succinate Dehydrogenase A
SEM	Standard Error Mean
SH2	Src-Homology 2
SH3	Src-Homology 3
SOS	Son-of-sevenless
TBST	Tris-buffered saline tween
TBST	Tris-Buffered Saline Tween
TCA	Tricarboxylic Acid
TEM	Transmission Electron Microscopy
Tm	melting temperature
TNM	Tumor, Lymph nodes, and Metastases
UV	Ultraviolet
V	Volt
V600	Valine 600
V600E	Valine to Glutamate Substitution

Table of contents

1. Introduction

1.1. Mitogen-activated protein kinase (MAPK) signaling pathways

1.1.1. Effectors of the MAPK signaling pathways

Mitogen-activated protein kinase (MAPK) pathways are central signaling pathways regulating fundamental cellular processes, including proliferation, differentiation, and stress responses[1]. Depending on many cellular and extracellular factors, three different sub-pathways can be activated (***Figure 1***). First, is the MAPK-ERK1/2 pathway, involved in cell proliferation and apoptosis. The second is linked to the activation of c-Jun N-terminal protein kinase (JNK) and is initiated in response to stress or the presence of lipopolysaccharides. The third pathway is induced by UV irradiation, inflammatory cytokines, or hypoxia, and induces activation of the p38 protein kinase[2,3].

Our work is focused on the MAPK-ERK1/2 pathway, a cellular signaling pathway primarily triggered by the activation of growth factor receptors (GFR) (***Figure 2***). GFR are characterized as receptor tyrosine kinases (RTK) composed of an N-terminal extracellular ligand-binding domain, a transmembrane domain, and a C-terminal intracellular part consisting of a tyrosine kinase domain. GFR are characterized by their specific activating ligand, such as epidermal growth factor (EGF) and fibroblast growth factor (FGF), for the epidermal growth factor receptor (EGFR) and fibroblast growth factor receptor (FGFR), respectively[4].

In detail, binding of EGF to its receptor leads to dimerization of two EGFR proteins and autophosphorylation of tyrosine residues within the intracellular domain[4]. Phosphorylated tyrosine residues then function as distinctive binding sites for proteins harboring the Src-homology 2 (SH2) domain, e.g. Growth factor binding protein 2 (Grb2) which contains one SH2 and two Src-homology 3 (SH3) domains[5]. The SH3 domain of the Grb2 protein binds the proline-rich region of the “son-of-sevenless” (SOS) effector, enabling its anchorage to the membrane. SOS is a guanine nucleotide exchange factor catalyzing the switch of guanosine diphosphate (GDP) to guanosine triphosphate (GTP), resulting in Rat sarcoma virus (RAS) activation[6].

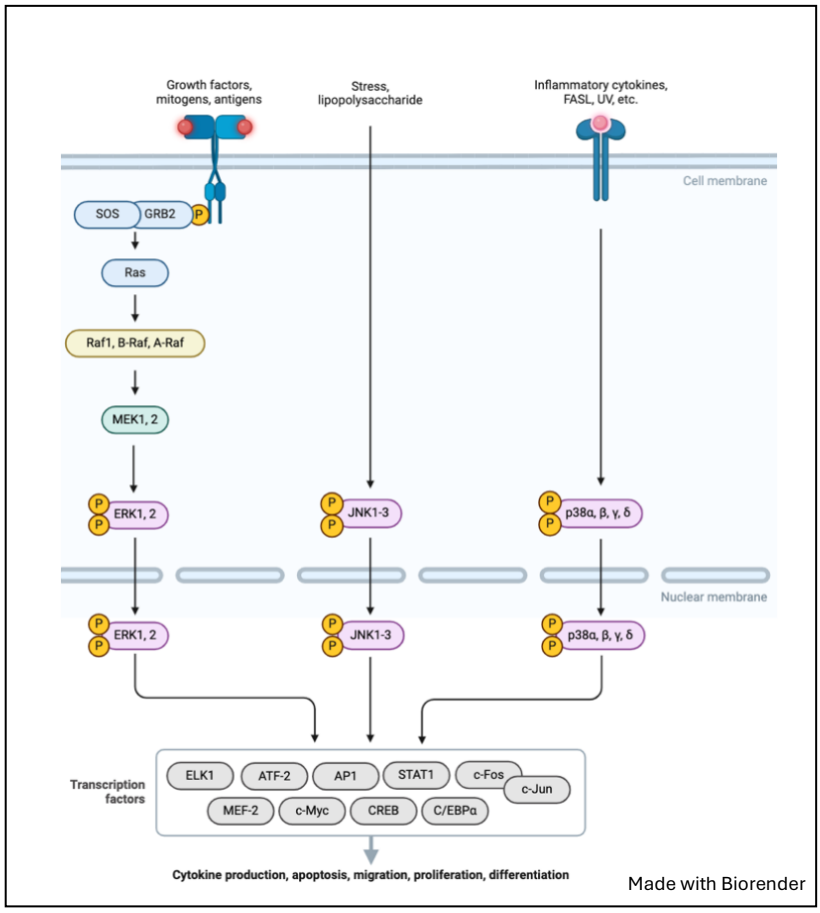

Figure 1: Representation of the three main MAPK pathways. Adapted from Jeffrey, K. L., *et al Nature Reviews Drug Discovery,* 2004.

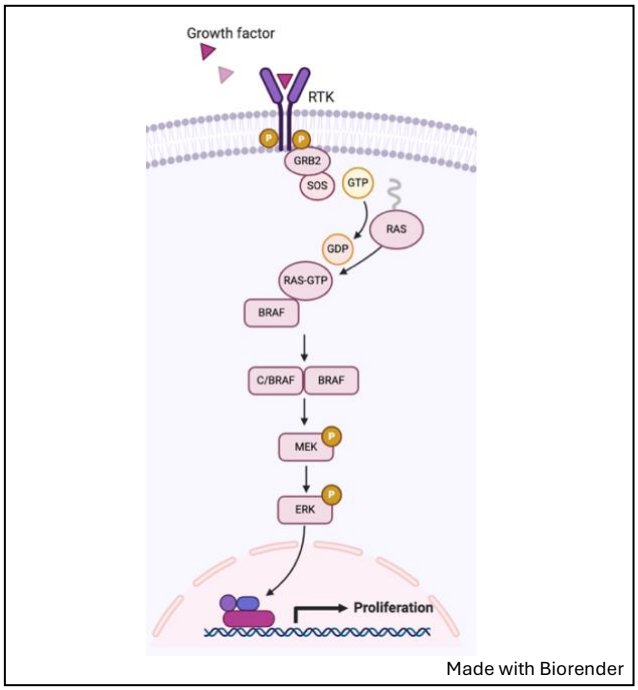

Figure 2: MAPK-ERK1/2 pathway

RAS proteins constitute a distinct family of small GTPases which include four members, K-RAS 4A, K-RAS 4B, N-RAS, and H-RAS. RAS proteins are involved in signal transduction via a switch from the inactive GDP-bound to the active GTP-bound form. RAS-GTP induces the activation of the rapidly accelerated fibrosarcoma (RAF) kinase family[5].

RAF represents a family of three different serine-threonine kinases, ARAF, BRAF, and CRAF, which share three conserved regions (CR) (***Figure 3***)[7]. CR1 is composed of a RAS-binding domain (RBD). The second conserved domain, CR2, is a serine-threonine-rich domain acting as a flexible hinge between CR1 and CR3. CR3, the third conserved region, is heavily involved in RAF activity. CR3 hosts the P-loop region responsible for ATP binding (***Figure 4***)[8]. Strong interaction between the P-loop region and the activation segment plays a crucial role in maintaining RAF in an inactive conformation. Under activating conditions, active RAS-GTP binds the RBD, resulting in RAF dimerization and phosphorylation. RAF kinases form both homodimers and heterodimers to achieve their full kinase activity[9]. RAF phosphorylation disrupts interactions between the P-loop and activation segment, flipping RAF into its active conformation[8], enabling RAF to phosphorylate and activate its downstream targets, MAP and ERK Kinases 1 and 2 (MEK1 and MEK2)[7, 9].

MEK family of protein kinases are characterized by their dual activity, whereby they can phosphorylate both tyrosine and threonine residues. Once activated by RAF, MEK1 and MEK2 phosphorylate extracellular-signal-regulated protein kinases 1 and 2 (ERK1 and ERK2), on tyrosine or threonine residues, resulting in their activation[10, 11, 12].

After its translocation in the nucleus, ERK it can act as a transcription factor or activate transcription factors leading to the expression of genes involved in cell survival, proliferation, apoptosis and metabolism[13]. For example, it has been demonstrated that ERK activation is necessary for cell cycle progression from G1 to S phase, notably via the regulation of cyclin expression (e.g. cyclin D1). In addition, ERK activation represses the expression of anti-proliferative genes, including p27, further highlighting the involvement of MAPK signaling in cell proliferation[14].

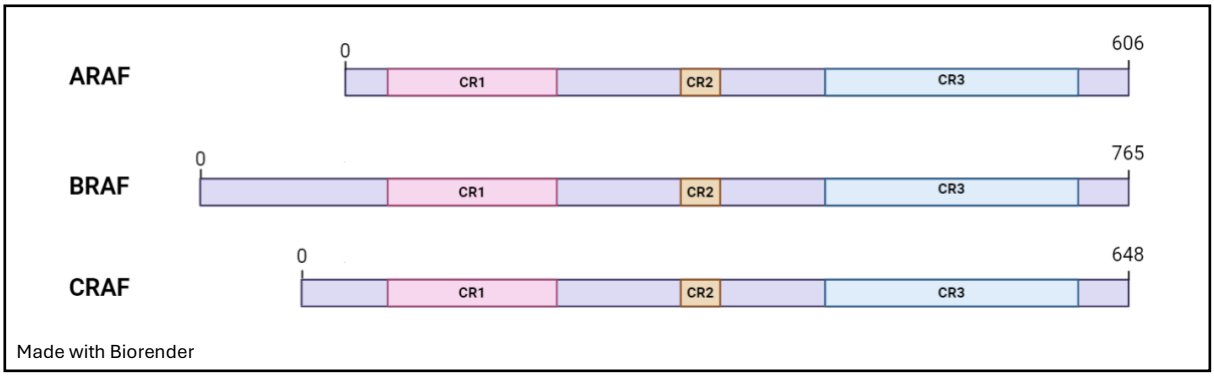

Figure 3: **Structure of the *RAF* isoforms, ARAF, BRAF and CRAF.** The RAF proteins share three conserved regions (CR): CR1 (pink), CR2 (orange) and CR3 (blue).

Adapted from Wellbrock, C., *et al Nature*, 2004.

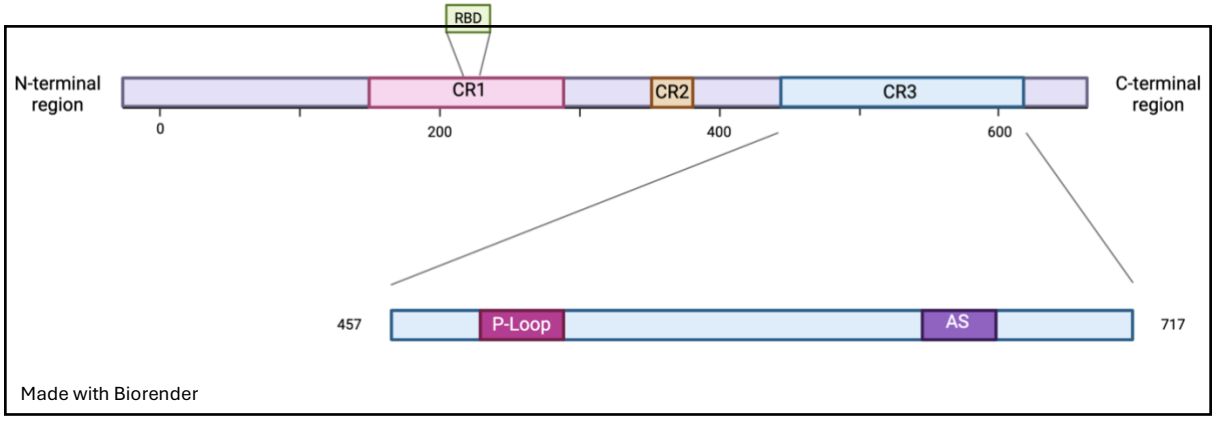

Figure 4: Schematic illustrating the domain structure of *BRAF*, including three conserved regions (CR). CR1 contains the RAS-binding domain (RBD) and CR3 contains the P-loop (enabling ATP binding) and activation segment (AS).

Adapted from Dankner, M., *et al Oncogene,* 2018.

Due to its fundamental involvement in crucial cellular functions, such as proliferation, differentiation and survival, the MAPK-ERK signaling pathway has been associated with the development of many human diseases, including cancer. Indeed, constitutive activation of the RAS-RAF-MEK-ERK pathway is a frequent event in many human cancers, arising as a consequence of mutations or genetic alterations in essential components of this pathway[15]. Of note, the RAS-RAF-MEK-ERK pathway is the most mutated cellular signaling pathway in cancer, with *KRAS* being the most common oncogenic gene driver in human cancers. In parallel, alterations within the *BRAF* gene also trigger uncontrolled cell proliferation, resulting in the onset and progression of cancer[16].

1.1.2. BRAF genetic alterations

BRAF mutations are found across a range of different cancers, in contrast, *ARAF* and *CRAF* mutations are far less frequent in cancer[17]. Three major classes of *BRAF* mutations have been defined: class I, II and III (***Figure 5***). Class I mutations occur at amino acid Valine 600 (V600) and activate MAPK signaling independently of RAS. Furthermore, class I mutations enable constitutive kinase activity of BRAF monomeric form. Non-V600 mutations are categorized as class II and III mutations. Class II *BRAF* mutations lead to functional, RAS-independent, BRAF dimers. Finally, class III mutations are characterized by reduced kinase activity, and require both upstream RAS activation and dimerization with wild-type RAF proteins. These three distinct classes of *BRAF* mutations serve as predictors for the efficacy of targeted therapies and hold significant implications for future drug development[8, 16].

1.1.2.1. $BRAF^{V600E}$ mutation

During my master thesis, my work focused on the $BRAF^{V600E}$ mutation. This V600E (valine to glutamate substitution) amino acid missense mutation, caused by a 1796T→A transversion in exon 15 of *BRAF*, represents the most predominant *BRAF* mutation, accounting for 80% of mutations identified in *BRAF*-mutated melanoma patients[18]. BRAF proteins carrying the V600E mutation have been shown to have a 500-700-fold increase in kinase activity compared to wild-type BRAF[19].

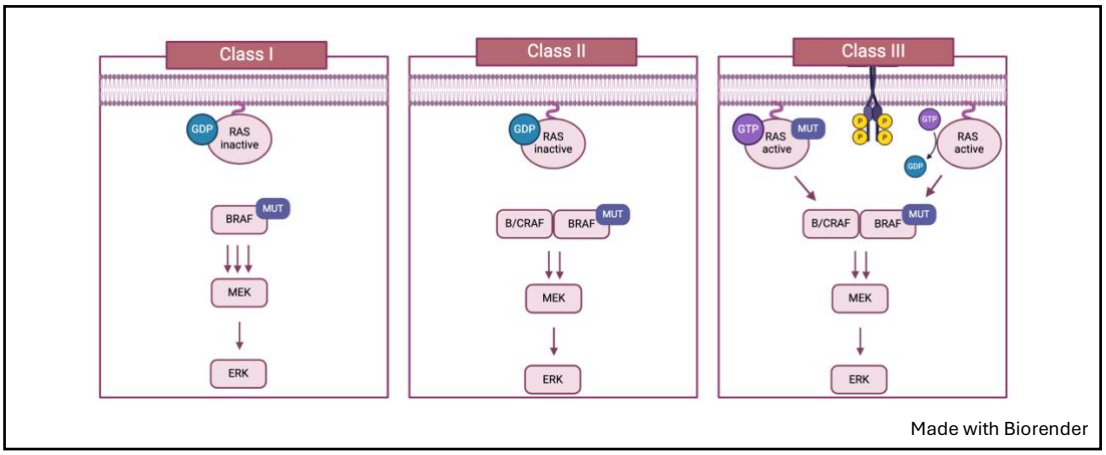

Figure 5: **Classification of *BRAF* mutations**. Adapted from Tabbò, F., *et al Cancer treatment reviews*, 2022.

The replacement of valine by a negatively charged glutamate mimics the negative charge usually brought about by RAS-mediated phosphorylation at threonine 598 and serine 601 within the activation segment[20], resulting in constant activation of the BRAF protein[18].

1.2. Cancers bearing BRAF^{V600E} mutation

The *BRAF*^{V600E} mutation is detected across a spectrum of solid cancer types encompassing melanoma, lung cancer, colorectal cancer and thyroid cancer. Among these cancers, melanoma, the most aggressive and invasive skin cancer, exhibits the highest frequency of the *BRAF*^{V600E} mutation. Indeed, half of melanomas have *BRAF* mutations, and importantly, as mentioned above, 90% of melanomas bearing *BRAF* mutations are V600 mutants[18]. The second most commonly BRAF mutated cancer is papillary thyroid cancer, one of the most common endocrine cancers. Between 40 and 60% of papillary thyroid carcinomas have a *BRAF*^{V600E} mutation. Interestingly, it has been shown that the presence of *BRAF*^{V600E} is correlated with an increased risk of recurrence, and thus, could represent a predictive biomarker for disease progression[21]. In addition, BRAF mutations are also detected in colorectal cancers, which rank third among the most frequently diagnosed malignant tumors. Indeed, approximately 10% of colorectal cancers harbor the V600E mutation and its detection serves as an indicator of poor prognosis[22]. Finally, the fourth cancer subtype bearing BRAF mutations is lung cancer. Lung cancers can be divided into two main categories based on cellular morphology and origin (***Figure 6***): small-cell lung cancer (SCLC) and non-small-cell lung cancer (NSCLC). NSCLC accounts for approximately 85% of lung cancers and can be further subdivided into 3 different subtypes: lung adenocarcinoma (LUAD), lung squamous cell carcinoma and large-cell carcinoma. Among LUAD, *BRAF* mutations are found in 3 to 8% of cases, with V600E accounting for half of the *BRAF* mutant LUADs (***Figure 7***)[23, 24]. Unlike the other cancer subtypes, *BRAF* mutant NSCLC is characterized by their equal distribution between V600 and non-V600 mutations, thus indicating a high prevalence of non-V600 mutations in this cancer subtype[25].

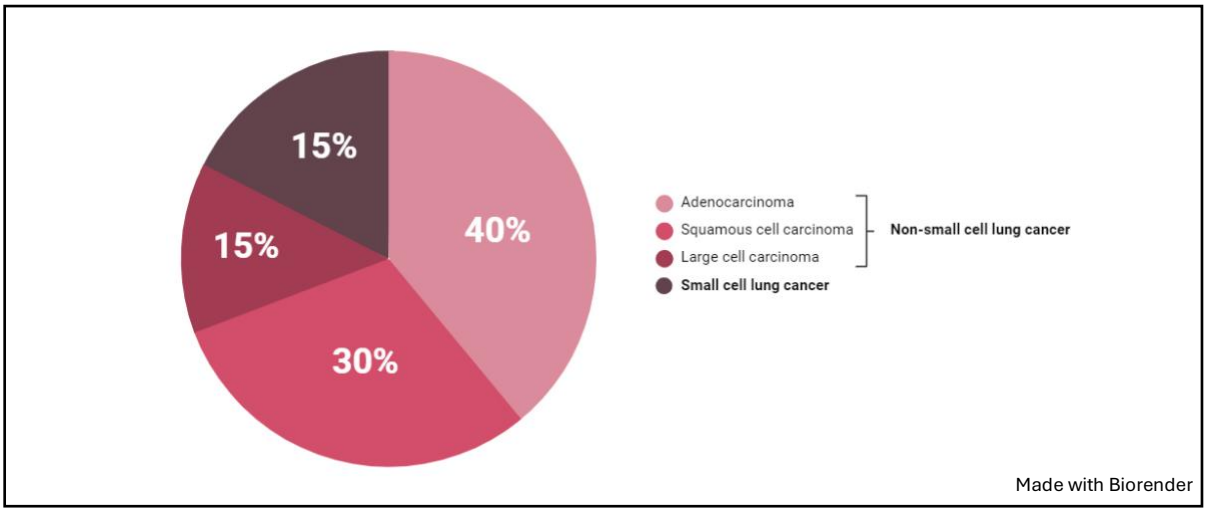

Figure 6: Lung cancer classification

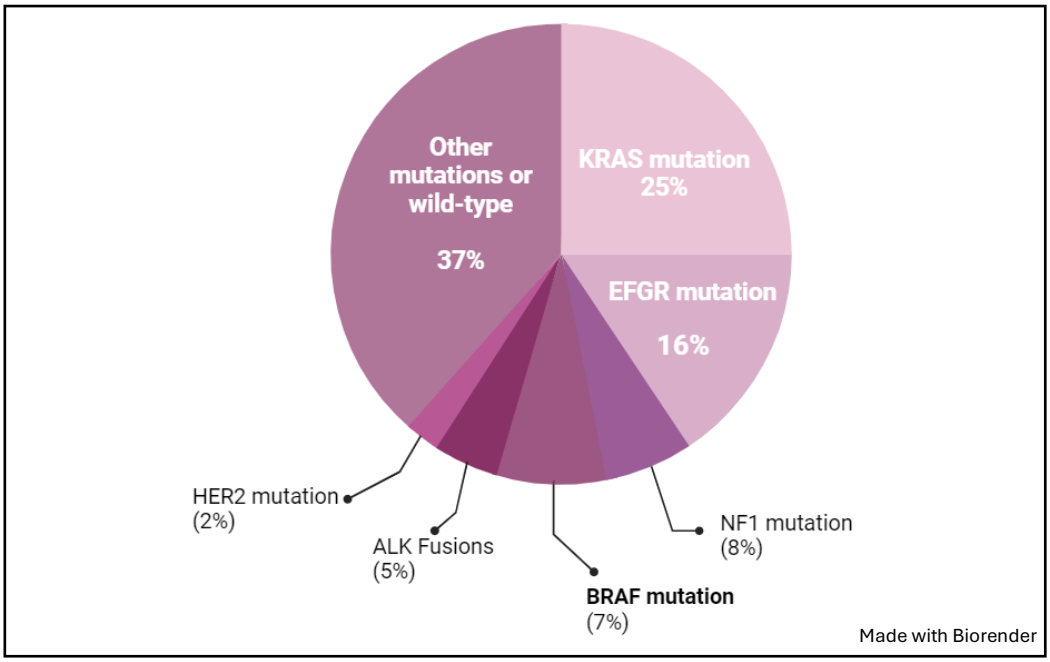

Figure 7: Frequency of driver mutations among lung adenocarcinomas. Adapted from Rosell, R. *et al, Lancet*, 2016.

1.2.1. Lung cancer

1.2.1.1. Epidemiology

In 2022, lung cancer stood out as the most prevalent and deadly cancer, with nearly 2.5 million new cases and 1.8 million deaths[26]. Fortunately, in developed nations, stringent smoking regulations have contributed to a gradual and steady decline in incidence rates. However, the opposite trend is observed in other regions like South America, Eastern Europe, and China, where incidence rates are unfortunately increasing[27].

1.2.1.2. Risk factors

Tobacco smoke emerges as the primary global risk factor, with roughly 80% of male and 50% of female lung cancer cases being attributed to current or prior smoking habits. Importantly, the association between adenocarcinoma and smoking is lower than that of the other types of lung cancer such as SCLC and squamous cell carcinomas. Accordingly, no correlation has been identified between smoking status and the occurrence of NSCLC with the V600E mutation, leading to the observation that this form of cancer predominantly affects non-smokers[28]. Additional risk factors for lung cancer include second-hand smoking, a family history of lung cancer and exposure to chemicals and pollutants like radon and diesel particles.

1.2.1.3. Anatomopathology

Beside the determination of the histological subtype (NSCLC vs SCLC), anatomical staging is a critical step in the evaluation of patients with lung cancer. Accurate staging is based on scores representing the extent of primary tumor size (T), infiltration of regional nodes (N) and metastatic dissemination to distant organs (M). TNM scoring is the common language for communicating the extent of disease and is fundamental to determining the most appropriate treatment strategy. In addition to TNM, molecular and immunological information are also considered for the diagnosis, to provide the most personalized therapeutic approach for each patient. Indeed, genetic alteration screening by next-generation sequencing and evaluation of immune checkpoint expression, are routinely performed for lung cancer patients[29].

1.2.2. Melanoma

Skin cancers are divided into two major categories, melanoma and non-melanoma. Melanoma is the most serious and least predictable skin cancer, accounting for only 1% of skin cancers, but responsible of 80% of deaths from skin tumors[30]. In most cases, melanoma develops in the skin, however, in rare cases, it manifests in the oral cavity, intestines, or ocular region. This latter, also known as uveal melanomas, originate in the eyes and account for 13% of all melanoma-related deaths. While half of cutaneous melanomas exhibit a *BRAF* mutation, uveal melanomas are notably devoid of this genetic alteration[31].

Non-melanoma skin cancers, like basal cell carcinomas and squamous cell carcinomas, are associated with a good prognosis, since they are often detected at early stages[32].

1.2.2.1. Epidemiology

Melanoma ranks as the fifth most prevalent cancer in both males and females, constituting approximately 4% of newly diagnosed cancers annually and contributing to 1.3% of all cancer-related deaths in Europe[33]. The incidence rate of melanoma has recorded one of the sharpest increases among all cancers, especially in developed countries and in fair-skinned populations. For example, in the US, between 1975 and 2018, the incidence of melanoma increased by 320%[34]. This rise can be partly explained by changing habits related to ultraviolet (UV) exposure. Additionally, women are more affected by this increase because they are more likely to partake in activities that increase the risk of melanoma, such as voluntary exposure to artificial sunlamps[35].

1.2.2.2. Risk factors

Similar to other malignancies, the development of melanoma can be due to genetic alterations or environmental factors, or a combination of both. Regarding genetic factors, inherited phenotypic traits, such as fair skin, light or red hair, freckles, and light eye color, represent conditions in which there is a stronger risk of developing melanoma. Unsurprisingly, a familial history of melanoma represents a considerable risk for the development of this illness. Regarding environmental risks, exposure to ultraviolet rays is emerging as the main risk factor for the development of melanoma. Importantly,

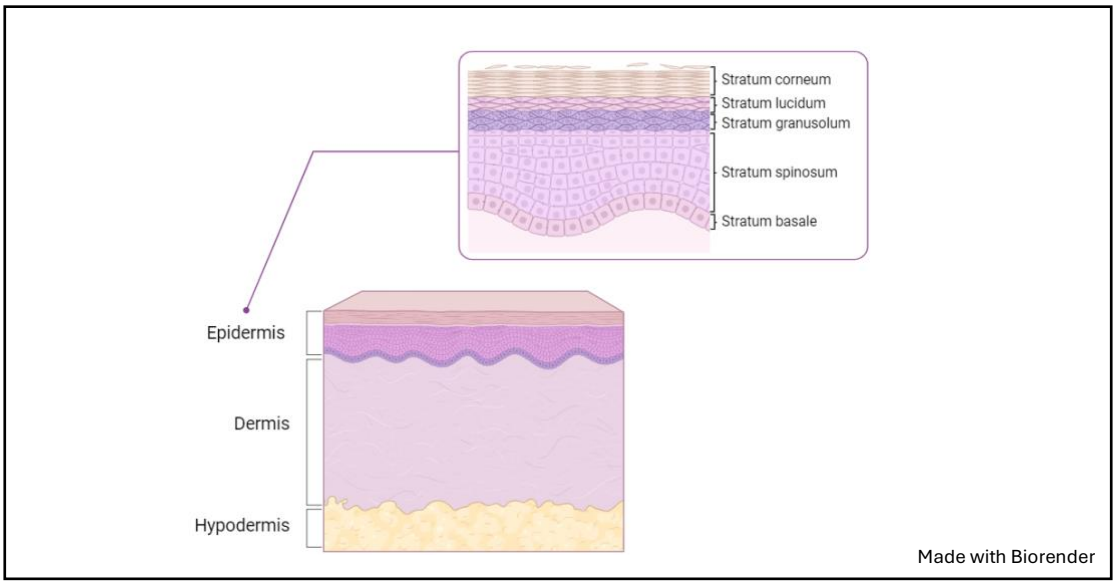

Figure 8: Schematic representation of the three main layers: epidermis, dermis and hypodermis, with a more detailed description of the sub-layers making up the epidermis.

UV exposure, as well as tobacco smoke (in the case of lung cancer), represent risk factors that can be avoided[32].

1.2.2.3. Pathophysiology and anatomopathology

Melanoma develops when melanocytes start to grow out of control. Melanocytes derive from the neural crest and are responsible for the production of a pigment, melanin, that protects the skin from UV radiation[31, 32]. These cells are located in the *stratum basal*, the deepest sub-layer of the epidermis (the external layer of the skin), as illustrated in ***Figure 8.*** Most melanoma deaths are linked to the presence of metastases, which can develop even from small primary tumors. Metastatic dissemination drastically reduces prognosis, reducing the median survival time to 6 months[36]. Most of the time, melanoma metastases are found in the lungs, brain, liver, and bones, while their presence in other locations is less frequent or rarely clinically observed[37].

Like for lung cancer, the different stages of melanoma are categorized based on tumor size, lymph node involvement, and metastatic dissemination (TNM) classifications. Accurate staging of melanoma is essential to assess patient prognosis and guide treatment decisions. As a result, an advanced stage is synonymous with a bad prognosis[38]. In addition to the TNM classification, two indexes can be used to assess melanoma severity. Firstly, the Clark level, classifies melanomas into five levels according to their depth of invasion into the skin. The second index, the Breslow depth, measures the thickness of the malignant tumor, specifically the distance between the most superficial layer of the skin, the epidermis, and the deepest part of the tumor. Of the two indices, the Breslow depth is more commonly used, as it is more specific. However, both indices remain important tools in the evaluation of melanoma, providing essential information for patient prognosis and treatment[39].

1.2.2.4. Treatments

In melanoma, the initial diagnosis is performed on a small skin biopsy. If the tumor is superficial and small, a surgery consisting of the complete removal of cancer cells with an adequate safety margin is performed[40]. In the case of advanced and metastatic disease, melanoma patients can be treated with a variety of anti-cancer modalities,

Table 1: Table summarizing the various advantages and disadvantages of cancer therapies.

	Advantages	Disadvantages
Surgery	• Often allows complete removal of localized cancer • Can be curative for cancers at an early stage	• Can lead to surgical complications (infections or bleeding • Not possible for cancers that have spread to surgically inaccessible locations
Chemotherapy	• Can destroy cancer cells throughout the body • Can be used in combination with other treatments to enhance effectiveness	• May damage healthy cells • May require multiple treatment cycles over an extended period • Can cause significant side effects
Radiotherapy	• Can cancer cells by specifically targeting the affected area • Can be used to treat unresectable tumors or to shrink a tumor before surgery as neoadjuvant therapy • Side effects are often limited to the treated area	• May require multiple sessions over an extended period • May damage health tissues closed to the irradiated area
Immunotherapy	• Specially target cancer cells while preserving healthy cells • Effective across a range of cancer types • May have fewer side effects than traditional chemotherapy	• Can lead to severe autoimmune side effects • Can be expensive • Low response rates but longer response (require the identification of biomarkers) •
Targeted therapies	• Specially target cancer cells while preserving healthy cells • Precision treatment based on genetic mutation	• Often leads to the development of resistance • High response rate but long-term effectiveness limited

including chemotherapy, radiotherapy, immunotherapy, and targeted therapies each with its advantages and disadvantages as described in ***Table 1***.Melanoma patients are treated in the first instance either with immunotherapy, targeted therapy, or a combination of the two. Targeted therapies are discussed in more detail in the following section.

Immunotherapy entails the use of antibodies to block immune checkpoints. Several immune checkpoint blockers are now approved for the treatment of melanoma patients, including pembrolizumab (Keytruda®), nivolumab (Opdivo®) and ipilimumab (Yervoy®). Ipilimumab, the first FDA-approved anti-CTLA-4 antibody for melanoma treatment, enhances T cell activity by specifically obstructing the CTLA-4 inhibitory signal. This action enables T cells to proliferate and infiltrate the tumor, ultimately resulting in tumor cell death[41].

1.3. Targeted therapy for BRAF mutated cancers

Targeted therapy involves the administration of drugs, such as small molecules or antibodies, designed to target specific proteins. Small molecule agents usually have a molecular weight below 900 Daltons and can penetrate the cell membrane[42]. Targeted therapies are mainly designed to target oncogenic mutated/altered proteins, with the aim of inhibiting the proliferation and dissemination of cancer cells and exerting limited effect on healthy cells. Thanks to their specificity, these drugs usually induce a high response rate in tumors bearing the altered target. However, as described below, the response is often limited due to the development of resistance.

1.3.1. Small molecules targeting the MAPK pathway: focus on BRAF and MEK inhibitors for BRAF mutated tumors

As mentioned above, deregulation of effectors of the MAPK pathway can lead to excessive signaling associated with aberrant cell proliferation and cancer. Therefore, targeting these deregulated kinases represents an appropriate therapeutic approach for preventing abnormal cell growth. Several small molecule inhibitors targeting MAPK effectors have been developed in the recent years. These drugs considerably improve

patient survival and are now recognized as an effective line of treatment for many cancer patients[43]. For example, KRAS is frequently mutated in cancers, particularly in NSCLC, and its mutated form can be inhibited by targeted therapy. Indeed, in May 2021, the Food and Drug Administration (FDA) approved the use of Sotorasib (Lumykras), a specific $KRAS^{G12C}$ inhibitor, to treat adult patients with KRAS-mutated NSCLC who have already received systemic therapy[44].

For my master thesis project, I focused on BRAF and MEK inhibitors, key treatments for BRAF-mutated lung and melanoma cancers. In particular, the combination of BRAF and MEK inhibitors has become one of the most effective targeted therapy combinations for BRAF mutant cancers[45]. Employing small molecule inhibitors that act on multiple effectors within the same signaling pathway has improved their efficacy compared to monotherapies; notably, by decreasing the likelihood of resistance development. As described below, monotherapies targeting crucial oncogenic signaling pathways frequently result in the acquisition of upstream or downstream activating mutations that render the treatment ineffective.

1.3.1.1. BRAF inhibitors

Various BRAF inhibitors (BRAFi) have been developed and commercialized over the past decade (***Figure 9***). Vemurafenib, marketed under the brand name Zelboraf, is an ATP-competitive inhibitor of mutant BRAF. It was the first BRAF inhibitor approved by FDA for treating $BRAF^{V600E}$-mutated metastatic melanoma, representing a pivotal advancement in precision medicine for this aggressive form of skin cancer[46]. Other BRAF inhibitors were subsequently developed and approved by the FDA. Dabrafenib (Tafinlar, GSK-2118436) is a reversible ATP-binding site competitive inhibitor of the V600 mutated form of BRAF. Dabrafenib has been shown to inhibit the phosphorylation of ERK, thus preventing ERK nuclear translocation and the transcription of target genes involved in cell proliferation[47]. In a phase III clinical trial of patients with *BRAF*-mutated metastatic melanoma, the efficacy of Dabrafenib was compared to dacarbazine, a chemotherapeutic frequently used to treat melanoma patients. Dabrafenib was shown to be more effective, with a progression free survival of 5.1 months compared to 2.7 months for dacarbazine[48].

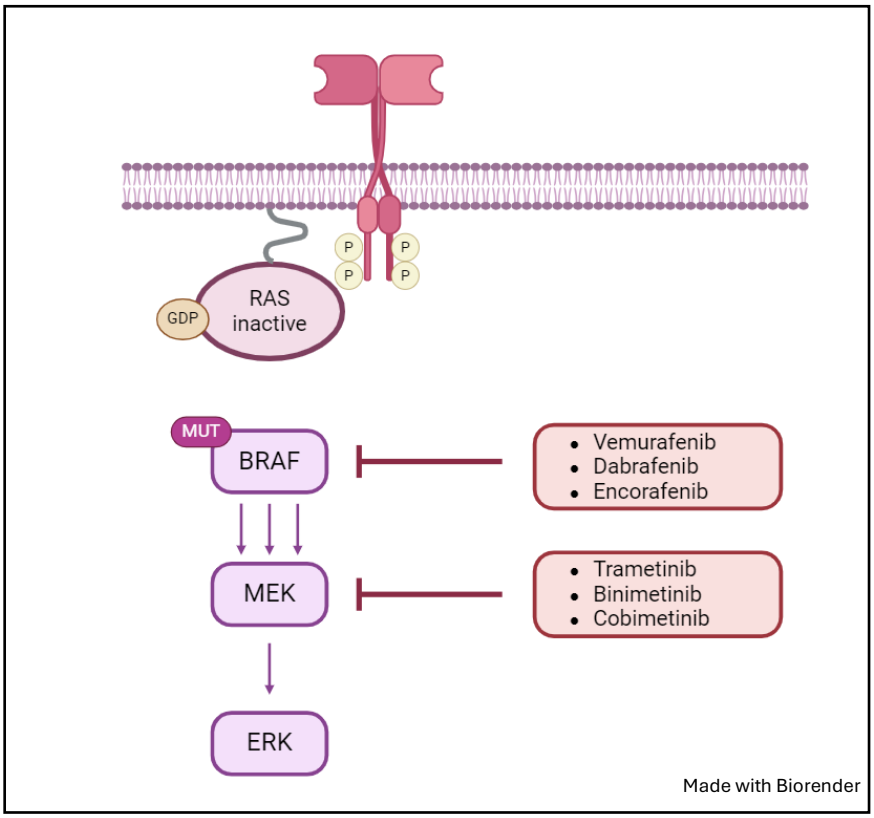

Figure 9: Scheme highlighting MAPK inhibitors, specifically BRAF inhibitors (Vemurafenib, Dabrafenib, Encorafenib) and MEK inhibitors (Trametinib, Binimetinib, Cobimetinib).

Encorafenib (Braftovi) is a potent and highly selective ATP-competitive inhibitor of BRAF. Encorafenib in combination with Binimetinib, was approved by the FDA in 2018, for the treatment of unresectable or metastatic BRAF mutant melanoma, and it received further approval in October 2023, for the treatment of metastatic *BRAF*^{V600E} NSCLC, also in combination with Binimetinib[49, 50].

1.3.1.2. MEK inhibitor

In addition to targeting BRAF, small molecule inhibitors specifically inhibiting MEK1 and MEK2, the downstream substrates of BRAF, have been developed, including Trametinib (Mekinist), Binimetinib (Mektovi) and Cobimetinib (Cotellic) (***Figure 9***). In 2013, Trametinib became the first drug approved by the FDA as a monotherapy for the treatment of V600 mutant metastatic or unresectable melanoma[51]. These inhibitors are non-competitive ATP inhibitors of MEK1 and 2. By binding to an allosteric site, it modifies the conformation of these kinases, impairing their kinase activity and the downstream signaling pathway activation[52]. The drawback of these MEK inhibitors is the lack of specificity towards cancer cells. Mutations in MEK1/2 are uncommon in human cancer, and consequently, MEK inhibitors may not selectively target MEK in cancer cells over normal cells, inducing the risk of normal tissue toxicity[53].

1.3.1.3. Combination of BRAF and MEK inhibitors

In *BRAF*-mutant melanoma, the predominant resistance mechanism to BRAF inhibitors is the reactivation of the MAPK pathway, leading to clinical studies testing the vertical double blockage of this pathway[54]. Indeed, it has been shown that treating *BRAF*^{V600E} melanoma with BRAF and MEK inhibitors, in combination, increases the treatment efficacy by improving the overall survival (OS) of patients. A phase III clinical trial (NCT01584648), reported that melanoma patients treated with Dabrafenib and Trametinib (D/T) in combination showed a 3-year OS and progression-free survival (PFS) of 44% and 22% respectively, compared with an OS of 32% and a PFS of 12% in patients treated with Dabrafenib monotherapy. Since 2018, this combination of drugs is the standard-of-care for *BRAF*-mutant melanoma[55]. The management of BRAF mutant lung cancer has been greatly impacted by the results observed in BRAF-mutant melanoma.

In 2016 and 2017, the first clinical reports showed robust anti-tumor activity of D/T in patients with *BRAF*^{V600E} mutant LUAD[55, 56]. Later, a 5-year survival update from the phase II study (NCT01336634) confirmed that for LUAD patients, D/T combination exhibited significant and long-lasting clinical advantages, along with a tolerable safety profile, regardless of prior therapies received. Clinical responses were similar between treatment-naïve and previously treated patients, with an overall response rate (ORR) of 63.9% and 68.4%, and a median PFS of 10.2 and 10.8 months, respectively. Following these results, in 2017, the FDA granted approval of D/T combination in metastatic *BRAF*^{V600E} NSCLC, independent of previous therapeutic treatments[57]. Later, in June 2022, the FDA granted accelerated approval of D/T for any *BRAF*^{V600E} unresectable or metastatic solid tumors in adult and pediatric patients (≥6 years old)[58]. Finally, as described above, a second combination with Encorafenib and Binimetinib has also been FDA approved for the treatment of BRAF mutated melanoma and lung cancer.

1.4. Resistance to targeted therapies

Resistance to targeted therapy is one of the greatest challenges faced by precision oncology. This resistance can be simplistically categorized as primary or acquired resistance. Indeed, primary resistance, also known as intrinsic resistance, refers to the inherent resistance of cancer cells to a particular targeted therapy. In a clinical setting, patients with intrinsically resistant tumors are referred to as non-responders, as their tumor volume does not decrease after the start of treatment. Conversely, acquired resistance refers to tumors that initially respond to targeted therapy, but during prolonged exposure to drugs show eventual relapse[59].

In melanoma, approximately 20% of patients undergoing treatment with BRAF inhibitors exhibit disease progression upon their initial evaluation, despite the presence of a *BRAF*^{V600E} mutation, indicating the presence of intrinsic resistance[60]. Pre-existing genetic mutations have been recognized as key factors contributing to intrinsic resistance following BRAF inhibition, in both preclinical models and clinical samples (e.g. PTEN loss, cyclin D1 amplification, RAC1 mutation among others)[61]. In particular, alterations in tumor suppressor genes like phosphatase and tensin homolog (PTEN),

are commonly detected in *BRAF* mutant melanoma. Interestingly, when compared to melanoma patients lacking PTEN alterations, patients with concomitant PTEN loss-of-function mutations tend to exhibit reduced OS and median PFS when undergoing treatment with BRAF and MEK inhibitors[62]. Acquired resistance, however, can develop via different processes. A common mechanism is the development of a secondary mutation within the target oncogene. For instance, the existence of an aberrantly spliced $BRAF^{V600E}$ isoform, known as p61*BRAF*(V600E), is associated with resistance to BRAF inhibitors. Specifically, this isoform lacks the RAS-binding domain , and demonstrates heightened BRAF dimerization in cells with low levels of RAS activation compared to $BRAF^{V600E}$, potentially contributing to drug resistance[61]. In parallel, resistance is frequently associated with the emergence of mutations that either reactivate the MAPK pathway or activate other bypass signaling pathways, making targeted therapy ineffective on cancer cells[63]. For example, it has been shown that melanoma cells acquire EGFR amplifications, leading to the development of resistance to BRAF and MEK inhibitors[64].

Nowadays, attempts at understanding mechanisms of resistance to BRAF and MEK inhibition is the subject of extensive research. The identification of resistant mutations represents a unique opportunity to provide an additional line of treatment targeting these resistance features. However, it has become apparent that resistance to targeted therapy is underpinned by early functional adaptations involving the rewiring of cell states and metabolic pathways. Actually, before this phase of resistance, cancer cells undergo a period of adaptation to the targeted therapies, entering a state of persistence that enables them to survive despite the pressure of treatment[65] (***Figure 10***). The concept and characterization of drug tolerant persister (DTP) cells is further described below.

1.5. Drug-tolerant persister (DTP) cells

1.5.1. DTP cells in microbiology

The concept of "drug-tolerant persister" (DTP) cells originated in the microbiology field, in the 1940s, during the discovery of antibiotics.

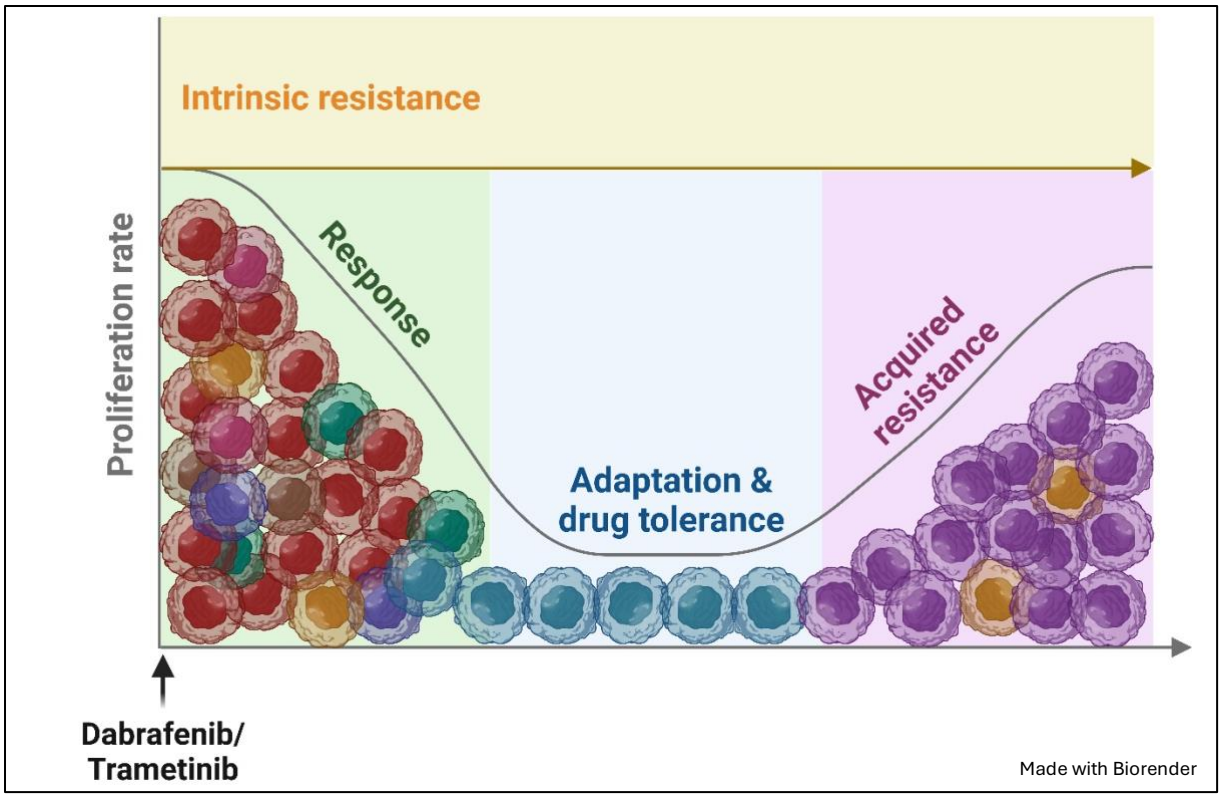

Figure 10: Resistance to targeted cancer therapies. Drug resistance can emerge during initial therapy (intrinsic resistance) or develop after initial therapy response (acquired resistance). Before this phase of resistance, cancer cells adapt to targeted therapies, entering a persistent state that allows them to survive despite treatment pressure. Adapted from Tangella, L. *et al, BBA*, 2021.

At that time, researchers observed that penicillin was capable of killing the vast majority of streptococcal cells, but a tiny quantity, around 1%, remained persistent. These cells were termed “bacterial persisters”[66]. In bacteriology, persistence is defined as “the capacity of a subpopulation of bacteria to survive exposure to antibiotics without undergoing *de novo* genetic alterations”[67]. Importantly, slow growth rate characterizes this persistent state, and furthermore, the withdrawal of the drug causes these tolerant cells to switch to a drug-sensitive state. Resensitization following drug withdrawal shows that this state of bacterial persistence is transient and mediated by phenotypic plasticity rather than genetic alteration[65].

1.5.2. DTP cells in cancer

In cancer, the term “persister” does not correspond to an exact biological definition and this term has different synonyms such as “tolerant” or “quiescent”. As globally accepted, persistent cancer cells have been defined as “a subpopulation of cells that survive initial anti-cancer treatment, showing a lower proliferative rate and surviving without *de novo* genetic mutations”. The distinction between these cells and resistant cells is that drug tolerant persister cells do not display mutational resistance mechanisms. Nonetheless, persistent cancer cells retain the ability to undergo mutations and could give rise to genetically modified resistant clones at a later stage[65].
Similar to bacterial persisters, cancer persisters can be distinguished by several major characteristics. Firstly, these cells remain viable despite the presence of the drug, by escaping drug-induced apoptosis for example[68]. Secondly, cancer persisters rely on slower cell cycling, enabling them time to facilitate metabolic changes and other survival mechanisms. Finally, the mechanisms implicated in cancer cell tolerance are non-genetic, meaning that the drug-persistent state is reversible and transient. A "drug washout" (also known as a "drug holiday") restores the sensitivity of the cells to the drugs. Thus, the major difference between persistent and resistant cells, is the fact that resistant cells have acquired genetic modifications, while persistent cells are considered as the reservoir from which genetically resistant cells can subsequently emerge[69, 70]. In addition, in our laboratory, we distinguish drug tolerant persister (DTP)

and drug tolerant expanded persister (DTEP), as cells which have been treated with D/T for 3- or more than 20-weeks,respectively (as detailed below). DTP are tolerant and slow proliferating cells, while DTEP are tolerant with slightly elevated proliferation compared to DTP cells.

1.5.2.1. Origins of DTP cells

There are currently two theories regarding the origin of "drug-tolerant persister" cells in cancer. According to the first, persister cells are present in the tumor even before treatment begins. Therefore, a subset of cancer cells with DTP characteristics exists, showing a selective ability to survive to drug exposure. As an example, transcriptional heterogeneity at the single-cell level has been demonstrated in *BRAF*-mutated melanoma cells, which is likely to predict which cells will resist drug therapy[71]. Meanwhile, other studies suggest that some persister phenotypes emerge through plasticity induced by drug treatment. Thus, exposure to therapy induces a phenotypic transition towards a state of tolerance. It is important to note that these two theories are not mutually exclusive[72].

1.5.2.2. Adaptations of DTP cells

In response to therapeutic stress, DTP cells undergo changes essential for their survival. These adaptations involve different processes such as epigenetic, transcriptional and translational modifications[73]. Persistent cells employ four main strategies to survive: slowing cell proliferation, modifying cell metabolism, changing cell identity, and interacting with the tumor microenvironment[65].

The focus of the current project is to investigate metabolic adaptations occurring in DTP cancer cells carrying the *BRAF*^{V600E} mutation, when exposed to D/T treatment.

1.6. Metabolic adaptations in BRAFV600E mutated melanoma after D/T exposure

During the 20th century, Warburg indicated that cancer cells utilize glucose to preferentially fuel glycolysis for ATP production, even in the presence of oxygen[74]. This energy production preference observed in cancer cells is commonly referred to as

"aerobic glycolysis." Interestingly, mutant BRAF constitutively activates the MAPK pathway, inducing the expression of genes involved in the regulation of energetic metabolism, such as hypoxia-inducible factor 1 α (HIF1α), which is a master regulator of glycolysis[75]. Thus, *BRAF* mutant melanoma cells usually present an enhanced glycolytic phenotype, associated with a high glucose uptake and an increased production of lactate[76]. Strikingly, several publications highlighted a metabolic switch in BRAF mutated cancer cells after D/T exposure. While treatment-naive melanoma cells tend to perform glycolysis, persistent cells shift towards mitochondrial oxidative respiration[77]. To achieve this metabolic adaptation, persister melanoma cells upregulate the expression of enzymes implicated in mitochondrial oxidative ATP production[78]. Therefore, energy production in slow-proliferating persistent cancer cells is more similar to that of resting normal cells, than to proliferating cancer cells[79].

To switch from glycolysis to oxidative phosphorylation, melanoma DTEP cells adapt their lipid metabolism by notably increasing fatty acid oxidation (FAO)[80]. This crucial energy-producing process, also known as β-oxidation, primarily occurs in the mitochondria and peroxisomes. During β-oxidation, fatty acids are progressively metabolized, resulting in the production of acetyl-CoA, NADH, and $FADH_2$, which subsequently feed into the TCA cycle and the electron transport chain (ETC)[81]. Persister melanoma cells enhance their fatty acid oxidation by significantly upregulating the expression of CD36, a key fatty acid transporter[82]. This adaptation allows for more efficient energy production, necessary for their survival under D/T treatment.

Moreover, the dependency on oxidative phosphorylation in *BRAF*^{V600E}-mutated melanoma cells following treatment with BRAF and MEK inhibitors involves a reduction in glucose consumption[83] and an increased reliance on glutamine to fuel mitochondrial metabolism. It has been shown that melanoma cells resistant to Vemurafenib utilize a higher amount of glutamine and exhibit increased sensitivity to glutamine deprivation compared to cells sensitive to MAPK inhibitors[84]. Thus, targeting glutamine metabolism could represent an alternative strategy for overcoming acquired resistance to MAPK inhibitors in melanoma.

Adaptation of mitochondrial metabolism in melanoma cells treated with targeted therapy was also shown to be regulated at the level of mRNA, whereby DTP cells adapt the nuclear export and translation of mRNA encoding for metabolic enzymes. Under.

pressure from BRAF-targeted therapy, the RNA processing kinase UHMK1 binds to mRNAs that encode metabolic proteins and preferentially regulates their translation and transport[85]. Thus, following therapeutic stress induced by BRAF inhibitors, selective mRNA transport and translation are activated, contributing to metabolic reprogramming.

1.7. Preliminary data in D/T persister BRAF mutated lung cancer cells

In parallel to melanoma findings, research projects in our laboratory focus on understanding the metabolic adaptations in *BRAF* mutant NSCLC cells, that are tolerant to D/T combination. In brief, our team has carried out a genome-wide CRISPR-Cas9 knockout screen on HCC364 $BRAF^{V600E}$ NSCLC cells treated with D/T (***Figure 11A***). After gene set enrichment analysis, it was clear that the expression of genes involved in metabolic pathways was significantly depleted in D/T-treated cells (***Figure 11B***). To further investigate metabolic adaptations in drug tolerant expanded persister (DTEP) cells, metabolite flux was measured in both parental and DTEP HCC364 cells using [U-^{13}C]-glucose, whereby the stable mass isotopomere distributions (MIDs) can be traced by mass spectrometry (LC-MS/MS). Results revealed that DTEP cells display a reduced tricarboxylic acid (TCA) cycle flux, whereas glycolytic flux was similar to parental cells (***Figure 11C***). Taken all together, these results highlight that DTEP cells are likely experiencing mitochondrial distress.

To better understand what happens at the mitochondrial level, confocal and transmission electron microscopy (TEM) were used to visualize the mitochondria. DTEP cells had altered mitochondrial localization and morphology with enlarged, hyperfused, and fewer mitochondria per cell (***Figure 11D***). Continuing in the same direction, mitochondrial activity was studied and revealed that DTEP cells exhibited decreased oxygen consumption rate (OCR) and NAD+/NADH ratio (***Figure 11E***). As DTEP cells present an altered mitochondrial activity, it is possible that DTEP cells would be sensitive to inhibition of the ETC. Synthesis of coenzyme Q10, a key electron carrier within the ETC, can be blocked using mevalonate pathway inhibitors, statins. As expected, statins decreased the viability and colony formation of HCC364 DTEP cells

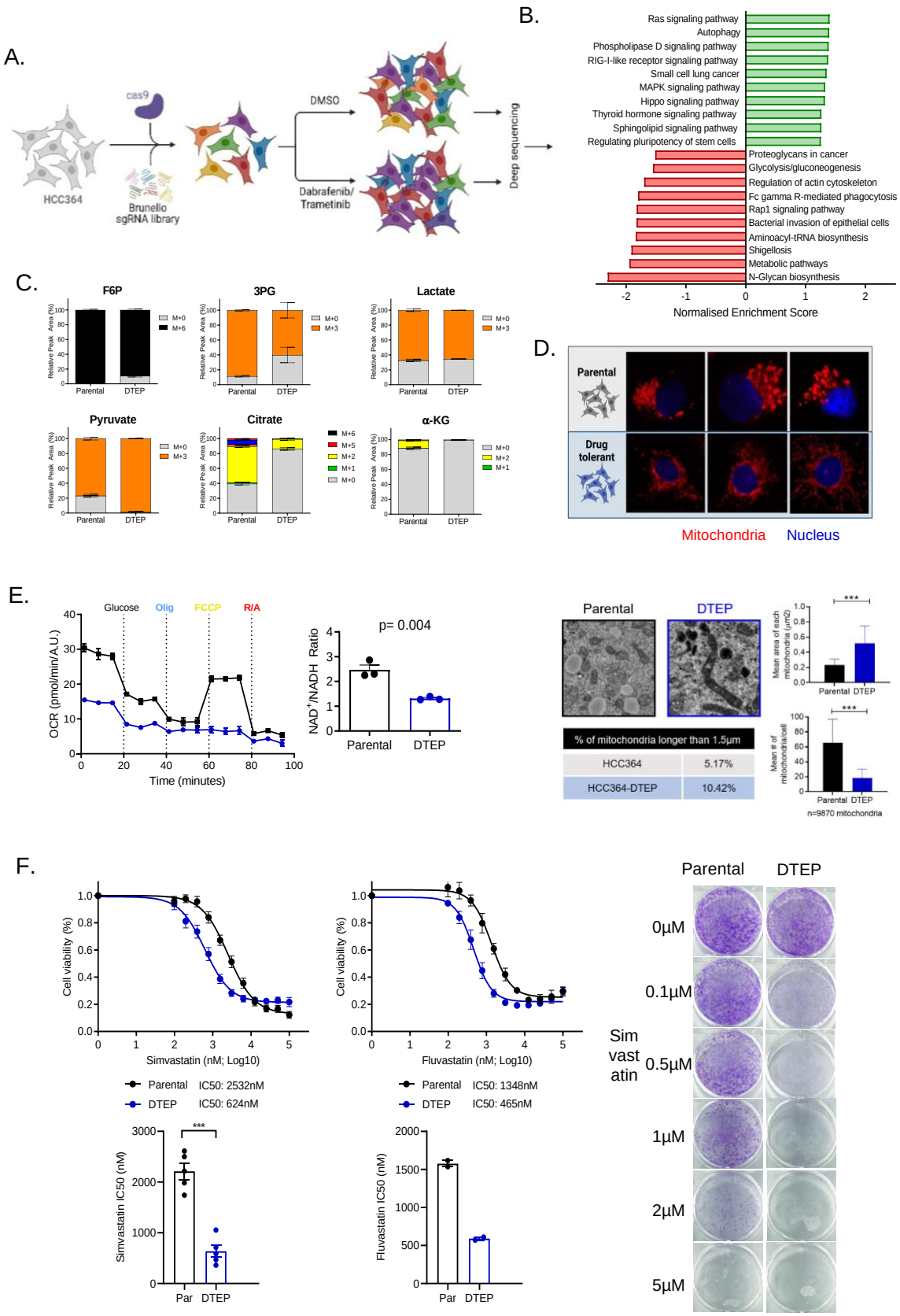

Figure 11. Preliminary data in persister lung cancer cells. See next page

more than parental cells (***Figure 11F***). Once again, these results suggest that HCC364 DTEP cells treated with the combination of D/T display mitochondrial dysfunction, and this vulnerability can be targeted with statins. These preliminary results seem at odds with what has been shown in the context of melanoma (as described above). Therefore, my master thesis project aimed at deciphering the metabolic adaptations of D/T persister melanoma cells generated under the same conditions as the LUAD models in our laboratory.

(A) Schematic showing workflow for genome-wide CRISPR-Cas9 knockout screen of D/T treated $BRAF^{V600E}$ NSCLC cells. (B) GSEA on significantly enriched and depleted genes ($p<0.05$) from genome-wide CRISPR-Cas9 knock-out screen of D/T treated cells. (C) Mass isotopomere distributions (MIDs) of glycolytic and TCA cycle metabolites from [U-^{13}C]-glucose stable isotope tracing in parental and DTEP $BRAF^{V600E}$ NSCLC cells. (D) Mitotracker red staining (confocal microscopy), transmission electron microscopy (TEM), and TEM quantification (mitochodrial size and number) in parental and DTEP $BRAF^{V600E}$ NSCLC cells. (E) Adapted mitochondrial stress test measuring oxygen consumption rate (OCR) and luminescence assay measuring intracellular NAD+/NADH ratio in parental and DTEP $BRAF^{V600E}$ NSCLC cells. (F) Statin (simvastatin and fluvastatin) IC50 analysis by MTT assay (72h) and colony formation assay (simvastatin) in parental and DTEP $BRAF^{V600E}$ NSCLC cells.

2. Objectives

Focusing on *BRAF*^{V600E} mutated lung adenocarcinoma (LUAD), one of the major research axes in the host laboratory aims at characterizing both (1) the energetic metabolism adaptations and (2) the subsequent targetable vulnerabilities acquired during unavoidable emergence of resistance to targeted therapies. The clinical objective is to eliminate the persister cells, from which aggressive resistant cells develop, in order to achieve long lasting clinical responses and provide an additional line of treatment for *BRAF*^{V600E} mutated tolerant/resistant LUAD patients. Interestingly, Dr Rebekah Crake has noted that *BRAF*^{V600E} persister LUAD cells exhibit compromised mitochondrial function after treatment with the current standard of care for these tumors (combination of BRAF and MEK inhibitors). Additionally, when exposed to statins, inhibitors of the mevalonate pathway, these persister cells demonstrate reduced viability and colony-forming capacity compared to parental cells. With this, Dr Crake identified metabolic adaptations as a new target to tackle drug tolerance in *BRAF*^{V600E} LUAD, whereby patients with drug-tolerant tumors could potentially benefit from switching therapy to FDA-approved statins.

However, these results are not in agreement with the existing literature, mainly focusing on *BRAF*^{V600E} mutated melanoma and using single BRAF inhibitor rather than the combination of BRAF/MEK inhibitors. Indeed, as mentioned above, several reports highlight an increased mitochondrial activity in these persister cells. Therefore, the main goal of my master thesis was to decipher the metabolic adaptations in melanoma cell lines, following the same procedure for generating the persister cells in the lung context. Indeed, the host laboratory generated drug tolerant expanded persister (DTEP) cells, by treating three commercial melanoma cell lines, A2058, A-375, and SK-MEL-1, with increasing doses of BRAF and MEK inhibitors (Dabrafenib and Trametinib) over multiple weeks. The **first objective** was to validate the “persister/tolerant” phenotype of the different BRAF^{V600E} melanoma DTEP cell lines. After, the **second objective** was to evaluate energetic metabolic adaptations of these melanoma DTEPs. Finally, the **third objective** was to evaluate the sensitivity to statins of these DTEP melanoma cells.

To achieve these objectives, cell culture as well as basic molecular biology techniques were used. Briefly, the DTEP phenotype of these cells was validated by evaluating their viability and proliferation post-drug holiday using both MTT assay and live cell imaging (Incucyte). Next, the adaptations of the energetic metabolism of DTEP cells compared with their parental untreated counterparts were evaluated. Firstly, mitochondrial activity was examined by XF-flux analysis using the Seahorse instrument. Mitochondrial quantification and localization were assessed using MitoTracker staining by flow cytometry and confocal microscopy, respectively. Western blot and qPCR techniques were then employed to evaluate protein and gene expression, respectively, of different effectors of glycolysis and TCA cycle. Lastly, the susceptibility to statins was evaluated by IC50 analysis, comparing viability of parental and DTEP cells using a MTT assay.

3. Materials and Methods

3.1. Cell culture

3.1.1. Cell lines

The A2058, A-375, and SK-MEL-1 cells (ATCC) were cultured in DMEM Dulbecco's Modified Eagle Medium (DMEM) medium containing 4.5g/L D-glucose, supplemented with 10% Fetal Bovine Serum (FBS), 1% penicillin/streptomycin and 2mM L-glutamine (***Table 2***) and maintained in an incubator at 37°C and 5% CO_2.

Table 2: Cell culture

Products	Company	Catalog number
DMEM (1x), 4,5 g/L D-glucose, no glutamine, and no pyruvate	Thermo Fisher Scientific	10938-025
L-glutamine 2mM	Merck	G1251
Penicillin – Streptomycin (10,000 U/mL)	Thermo Fisher Scientific	15140-163
Fetal Bovine Serum (FBS)	Thermo Fisher Scientific	12676029
0,05% Trypsin-EDTA (1x)	Thermo Fisher Scientific	25300-054

3.1.2. Development of persister cells

The generation of persister cells was performed prior to my arrival in the host laboratory. Briefly, the half maximal inhibitory concentration (IC50) of Dabrafenib (TargetMol, T8474) and Trametinib (TargetMol, T2125) were determined for all cell lines using a MTT assay (protocol described below). Then, drug-tolerant expanded persister (DTEP) cells were obtained by treating each cell line for 20 and 40 weeks, with increasing concentrations of Dabrafenib and Trametinib (D/T), starting for their respective IC50 up to the following concentrations:

- A2058: 1μM Dabrafenib and 100nM Trametinib
- A-375: 400nM Dabrafenib and 10nM Trametinib
- SK-MEL-1:1μM Dabrafenib and 100nM Trametinib

A2058-DTEP, A-375-DTEP and SK-MEL-1-DTEP cells were cultured in DMEM full medium supplemented with Dabrafenib and Trametinib, with replacement twice a week.

3.1.3. Drug holiday

To perform a drug holiday (DH), Dabrafenib and Trametinib were removed from the DTEP cells for 3 weeks. After this period, DH cells were rechallenged with the combination of Dabrafenib and Trametinib (at the concentration outlined in section 3.1.2.), and both viability and proliferation were evaluated using MTT assay and Incucyte, respectively.

3.2. Cell viability and proliferation assays

3.2.1. MTT (cell viability) assay

To quantify cell viability were seeded (2,000 cells/well) in a 96-well plate and treated with or without Dabrafenib and Trametinib (using concentrations outlined in Section 3.1.2.). On days 0, 1, 3, 6, and 7 of D/T treatment, 100μL/well of 1mg/mL Thiazolyl Blue Tetrazolium Bromide (MTT; Sigma, M2128-1G) solution (diluted in DMEM full medium), was added to the cells for 3 hours. Finally, 100μL of a solubilization solution, composed of 10% SDS and 0.01M HCl, was added to each well. Twenty-four hours later, the absorbance was measured using spectrophotometer and data were analyzed.

3.2.1. Incucyte (cell proliferation) assay

Cell proliferation was assessed in real-time using live imaging (Incucyte SX5). Parental and DTEP cells were seeded in a 96-well plate with 2,000 cells per well for A2058 cells and 1,000 cells per well for A-375 and SK-MEL-1 and treated with and without D/T (using concentrations outlined in Section 3.1.2.). Cell proliferation was followed every two hours for 96 hours and data were analyzed with the Incucyte software.

3.3. Metabolic flux analysis

To analyze and compare the mitochondrial activity of both parental and persister cells, a metabolic flux analysis using the Seahorse XF HS Mini Analyzer (Agilent, S7852A) was performed. The day before the experiment, parental and DTEP cells were seeded in

8-well plates (Agilent, 103025-100) with 10,000 cells per well for A2058 cells and 7,500 cells per well for A-375 and SK-MEL-1 cell lines, in 80 µL of DMEM full media. The day of the experiment, assay medium was prepared using 7mL of 'XF DMEM Seahorse' medium (Agilent, 103575-100) at pH 7.4, supplemented with 2µM L-glutamine and warmed to 37°C. DMEM medium (***Table 2***) was replaced by 180µL of assay medium, and the cells were placed in a CO_2-free incubator at 37°C for 45 minutes. The different compounds interfering with the ETC complexes (***Annex I***) were prepared according to the dilutions shown in ***Table 3***. The cartridge (***Figure 12***) was loaded as follows and placed in the instrument for calibration:

- 20µL glucose (1mM) in well A
- 22µL oligomycin (10µM) in well B
- 25µL FCCP (Carbonyl cyanide-4 trifluoromethoxy phenylhydrazone, 10µM) in well C
- 28µL rotenone (5µM) and antimycin A (5µM) in well D

Table 3: Dilutions of the molecules acting on electron transport chain complexes

Products	1st dilution	2nd dilution
Oligomycin	1µL stock solution + 251µL assay medium (50 µM)	60µL diluted stock solution + 240µL assay medium (10 µM)
Rotenone/ Antimycin A	1µL of each stock solution + 214µL of assay medium (25 µM each)	60µL diluted stock solution + 240µL assay medium (5 µM each)
FCCP	1µL stock solution + 287µL assay medium (50 µM)	60µL diluted stock solution + 240µL assay medium (10 µM)

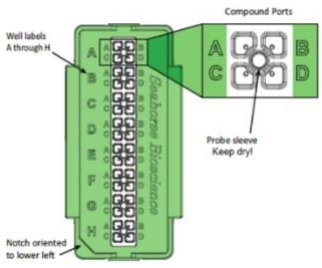

Figure 12: Cartridge used to load molecules acting on the electron transport chain

Following calibration, the cartridge was replaced by the 8-well plate containing the cells. All results were normalized to DNA quantification, measured by Hoechst staining

(Calbiochem, 382061) using the FilterMax F5 spectrophotometer (Multi-mode Microplate Reader, Molecular Devices) and SoftMax pro software.

3.4. Mitochondrial location and morphology analysis using MitoTracker staining

3.4.1. Cell seeding

To study the location and morphology of mitochondria, cells were stained using the MitoTracker Red CMXRos probe (Cell signaling, 9082). Coverslips previously sterilized with ethanol were placed in 24-well plates. Parental and DTEP A2058 cells were seeded (150,000 cells per well) in 1mL of DMEM full medium for 48h at 37°C and 5% CO_2.

3.4.2. Fixation, staining and visualization

A 1mM stock solution of MitoTracker® (Cell signaling, 9082) was prepared by diluting 50µg of powder in 94.1µL of dimethyl sulfoxide (DMSO, Roth, HN47.1). This stock solution was further diluted in DMEM full medium to obtain a final concentration of 200nM, and then incubated with the cells for 30 minutes at 37°C and 5% CO_2. The cells were then washed with phosphate-buffered saline (PBS) (composition described in ***Annex II***), fixed with 500µL of 100% ice-cold methanol for 15 min at -20°C. Fixed cells were washed 3 times with PBS, and nuclei were stained using DAPI solution (Invitrogen, H3570, diluted 1/2000 in PBS) by incubation for 30 min at room temperature in the dark. After an additional wash with PBS, the slides were mounted on microscope slides with 20µL of Fluoromount-G® (SouthernBiotech, 0100-01). Microscope slides were then stored at 4°C and protected from light until use with the confocal microscope. Images were acquired using the Leica SP5 confocal microscope with the 63x objective lens.

3.4.3. Quantification

The images obtained with the confocal microscope were used to study various parameters relating to mitochondrial morphology by performing quantification using the "MiNa" plugin in ImageJ (software version 1.54f).

3.5. Quantification of mitochondria by flow cytometry

A2058 parental and DTEP cells were seeded at 100,000 cells per well in 6-well plates (in DMEM full medium) and incubated at 37°C and 5% CO_2. DTEP cells were treated with cell line specific Dabrafenib and Trametinib concentrations outlined in Section 3.1.2. After 48h, cells were incubated with MitoTracker Green FM probe (Cell Signaling, 9074) diluted in DMEM full medium to a final concentration of 100nM for 30 minutes at 37°C. The cells were then trypsinized, centrifuged at 1,400 rpm for 5 minutes, and resuspended in PBS with 2% FBS. The cells were protected from light until flow cytometry analysis with the BD FACS Canto II instrument. The median fluorescence intensity (MFI) of each replicate of each condition was obtained using the following formula: (median fluorescence of the condition - median fluorescence of the unstained condition)/median fluorescence of the unstained condition.

3.6. Protein and RNA sample collection and preparation

Proteins and RNA were extracted from A2058 parental and DTEP cells treated for different time points (as indicated in the results section) with the combination of D/T at the concentrations described in section 1.2 (parental cells remained untreated). In a 6-well plate, 300,000 cells were seeded in 2mL of DMEM medium and incubated at 37°C and 5% CO_2.

3.6.1. Protein extraction and dosage

Protein extraction was carried out using 50µL of complete lysis buffer (CLB) (***Annex III***) composed of lysis buffer, phosphatase inhibitor, and protease inhibitor. Extracted proteins were quantified using the DC Protein Assay kit (Bio-Rad, 5000111). Bovine serum albumin (BSA, Merck, 82-045-2) solution, with concentrations ranging from 0.156 to 20mg/mL, was used as a standard curve. 3µL of protein sample or BSA standard was loaded in a 96-well plate. The DC Protein Assay kit reagents were then added to each well, according to manufacturer's instructions, and the plate was incubated for 15 minutes at room temperature in the dark. Absorbance was read at 750nm using the

the MultiScan FC (Thermo Fisher Scientific, 51119000) and SKanIt software.

3.6.2. RNA extraction and reverse transcription

RNA was extracted from the cells using the "NucleoSpin® RNA" extraction kit (Macherey-Nagel, 740955.50), following manufacturer's instructions. RNA quantity and purity were determined with the NanoPhotometer N50 (Implen). One microgram of RNA was then reversed transcribed into complementary DNA (cDNA) using the FastGene Scriptase II cDNA 5x ReadyMix (Nippon genetics, LS65). A negative control without the reverse transcriptase was also prepared. The samples were then incubated for 10 minutes at 25°C, 60 minutes at 42°C, and 5 minutes at 85°C in a thermocycler.

3.7. Real-time quantitative PCR

Real-time quantitative polymerase chain reaction (RT-qPCR) was used to quantify mRNA levels of genes of interest. To achieve this, cDNA was diluted 10x in RNase-free water. 2µL of diluted cDNA was mixed with 2.8µL RNase-free water, 6µL of 2X FastStart SyberGreen Master (Roche, 04673484001), and 0.6µL forward (20µM) and reverse (20µM) primers. The sequences of each primer pair are described in ***Table 4***. 18S housekeeping gene was used for normalization. RT-qPCR was then performed using a thermal cycler (QuantStudio3, Thermo Fisher Scientific - A28567), following the program described in ***Table 5***. Design & Analysis software (version 1.5.1) was used to calculate Ct (cycle threshold) values. Next, ΔCt was obtained by subtracting the Ct of the housekeeping gene from the Ct of the gene of interest. The difference between the ΔCt of the sample of interest and the ΔCt of the reference sample was calculated. Finally, the amount of target, normalized to the endogenous reference and relative to a reference sample, is given by the formula $2^{-\Delta\Delta CT}$.

Table 4 : Primer sequences

Gene	Forward sequence	Reverse sequence
mRNA		
SLC2A (GLUT1)	TCTGGCATCAACGCTGTCTTC	CGATACCGGAGCCAATGGT
PGK1	TGGACGTTAAAGGGAAGCGG	GCTCATAAGGACTACCGACTTGG
LDHA	ATGGCAACTCTAAAGGATCAGC	CCAACCCCAACAACTGTAATCT
SLC16A1 (MCT1)	AGGTCCAGTTGGATACACCCC	GCATAAGAGAAGCCGATGGAAAT
SLC16A3 (MCT4)	CGGCTTTGTGCTTTACGCC	GCTGAAGAGGTAGACGGAGTA
SDHA	CAAACAGGAACCCGAGGTTTT	CAGCTTGGTAACACATGCTGTAT
HMGCR	TGATTGACCTTTCCAGAGCAAG	CTAAAATTGCCATTCCACGAGC
18S rRNA	GCGGCGGAAAATAGCCTTTG	GATCACACGTTCCACCTCATC
Complex I subunits		
MT-ND1	GGCTATATACAACTACGCAAAGGC	GGTAGATGTGGCGGGTTTTAGG
MT-ND2	CTTCTGAGTCCCAGAGGTTACC	GAGAGTGAGGAGAAGGCTTACG
MT-ND4	CCCTCGTAGTAACAGCCATTCTC	CGACTGTGAGTGCGTTCGTAGT
MT-ND6	GCGATGGCTATTGAGGAGTATCC	CACAGCACCAATCCTACCTCCA
NDUFA1	ATGTGGTTCGAGATTCTCCCC	CCTGTGGATGTACGCAGTAGC
NDUFAB1	ATGGCGTCTCGTGTCCTTTC	AACCTGCGCGAGCACTAAG
NDUFB1	GTCCCTATGGGATTTGTCATTGG	CAGTTAGCCGTTCATCACTCTT
NDUFB8	CCGCCAAGAAGTATAATATGCGT	TATCCACACGGTTCCTGTTGT
NDUFC1	CCTTCAGTGCGATCAAAGTTCT	CAGCCAGTCAGGTTTGGCAT
NDUFS1	TTAGCAAATCACCCATTGGACTG	CCCCTCTAAAAATCGGCTCCTA
NDUFV1	AGGATGAAGACCGGATTTTCAC	CAGTCACCTCGACTCAGGGA

Table 5: RT-qPCR program

Step	Duration	Temperature	Modification of temperature (°C/s)	Cycles
Hold stage	10min	94°C	1.6	1
PCR stage	15s	94°C	1.6	45
	30s	60°C	1.6	
	20s	72°C	1.6	
Melt curve stage	5s	95°C	2.6	1
	1min	65°C	1.6	
	1s	94°C	0.15	
Post-read stage	15s	40°C	1.6	1

3.8. Western blot

Expression of selected proteins was quantified by Western blotting. All the solutions used are described in ***Annex IV***. 15µg of proteins were mixed with loading buffer (diluted 1 in 5) (***Annex IV***) and denatured for 5 minutes at 95°C. Denatured protein samples were loaded

into 8, 12, or 16% polyacrylamide gels (gel compositions are described in ***Annex V***). Proteins were then separated by migration through the gel, initially by electrophoresis at 100 volts (V) for approximately 30 minutes, followed by approximately 75 minutes at 120V. Separated proteins were then transferred on a polyvinylidene fluoride (PVDF; Thermo Fisher Scientific, 88518) membrane at 100V for 1 hour. Unspecific sites of the PVDF membrane were blocked with 5% milk [diluted in 1x Tris-buffered saline tween (TBST); ***Annex IV***] for 60 minutes under agitation and then incubated under agitation with the primary antibody solution overnight at 4°C. After three washes with TBST, membranes were incubated with the HRP-coupled secondary antibody for one hour at room temperature. All primary and secondary antibodies used are listed in ***Table 6***. After 3 additional washes with TBST, the chemiluminescent signal was revealed using the Clarity™ Western ECL Subrate kit (Bio-Rad,1705061) and acquired using the Amersham ImageQuant 800.

Table 6: Antibodies used for Western Blot

Target protein	Dilution	Host species	Company	Catalogue number
ACLY	1/1000	Rabbit	Cell Signaling	cs4332s
Fumarase	1/1000	Rabbit	Cell Signaling	cs4567s
GLUT1	1/1000	Rabbit	Cell Signaling	cs12939s
Hexokinase 2	1/1000	Rabbit	Cell Signaling	cs2867s
HSP 90	1/1000	Rabbit	Cell Signaling	cs4877s
Isocitrate dehydrogenase 1	1/1000	Rabbit	Cell Signaling	cs3997s
MPC2	1/1000	Rabbit	Cell Signaling	cs46141
NDUFB8	1/1000	Rabbit	Cell Signaling	cs73951s
pACLY Ser455	1/1000	Rabbit	Cell Signaling	cs4331s
PDH	1/1000	Rabbit	Cell Signaling	cs3205s
pPDH Ser293	1/1000	Rabbit	Abcam	ab92696
Succinate dehydrogenase A	1/1000	Rabbit	Cell Signaling	cs11998s
Total OXPHOS	1/1000	Mouse	Abcam	ab110411
B-Actin	1/1000	Rabbit	Cell Signaling	cs4970s
Anti-rabbit IgG, HRP-linked	1/3000	Goat	Cell Signaling	7074
Anti-mouse IgG, HRP-linked	1/3000	Horse	Cell Signaling	7076

3.9. Statistical analysis

All results were reported by the mean and Standard Error of the Mean (SEM). Unpaired t-test was used to compare two different groups. Multiple group comparisons were performed using one-way or two-way ANOVA depending on the number of grouping factors. Dunnet's test was applied for simple comparisons (one-way ANOVA) while Bonferroni's (two-way ANOVA) tests were used for multiple comparisons. In all cases, the difference between the two conditions is considered significant when the p-value is less than 0.05. GraphPad Prism (version 9.5) was used to generate graphs and perform statistical analyses.

4. Results

4.1. Validation of the persister phenotype in DTEP SK-MEL-1, A-375 and A2058 cells

As mentioned above, SK-MEL-1, A-375, and A2058 cells were treated with Dabrafenib and Trametinib (D/T) for several weeks until slow proliferating cells, referred to as drug tolerant expanded persister (DTEP) cells, were obtained. For the A2058 cells, two populations of DTEP cells were generated, the 20-and 40-week treated cells. To better confirm the "persister" phenotype of the different melanoma cell lines, a "drug holiday" (DH) or drug wash out was performed[86]. This procedure consists of removing the drug treatment for three weeks. After this period, the cells were rechallenged with the same combination of inhibitors and both the viability and the proliferation of these cells were assessed by MTT and Incucyte analysis, respectively. DTEPs would revert to a drug-sensitive state upon drug holiday, while the proliferation of resistant cells would not be affected by this rechallenge, indicative of acquired genetic mutations.

For the three cell lines, their respective parental cells were used as controls and showed a dramatically reduced proliferation rate when cultured in presence of D/T. In contrast, DTEP cells exhibited an intermediate proliferative phenotype between untreated and treated parental cells. As expected, DTEPs reverted to a drug-sensitive state upon removal of the D/T treatment (DH for 3 weeks), indicating that cell proliferation in the presence of the drugs was sustained by a non-mutational adaptive mechanism, and ultimately, confirmed the persister phenotype of our DTEP cells (***Figures 13 & 14***). Of note, no difference between 20- and 40-week DTEP A2058 cells was observed.

4.2. Mitochondrial activity is modulated in DTEP cells in a cell line dependent manner

The second objective of my project was to evaluate the mitochondrial activity of DTEP SK-MEL-1, A-375 and A2058 cells compared to their parental counterparts. We took advantage of the Seahorse cell metabolic analyzer (Agilent) which allows measurement

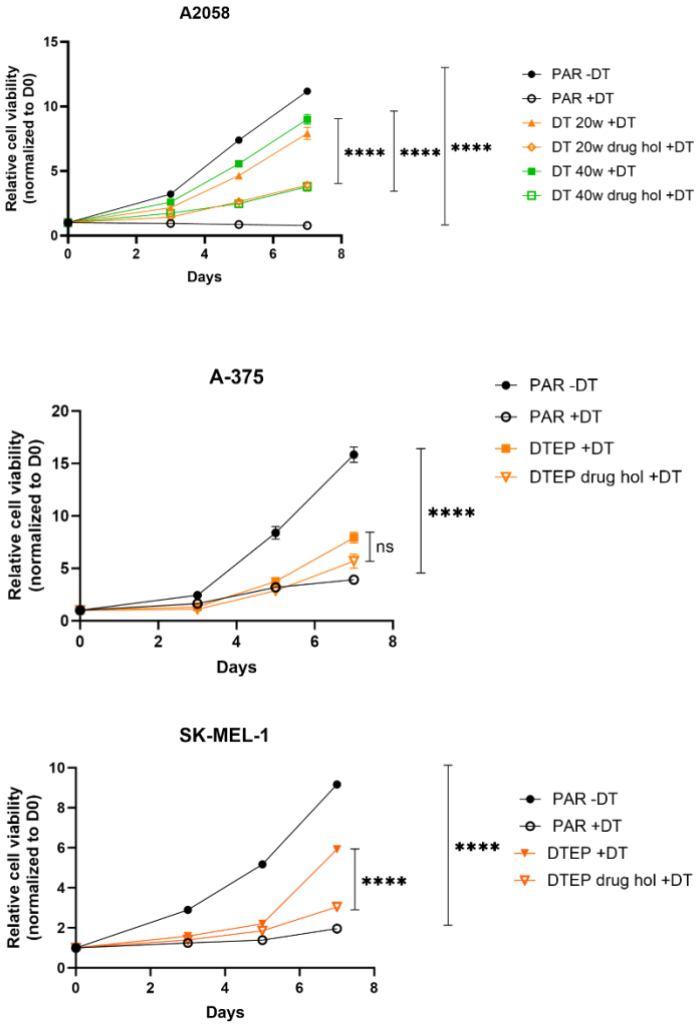

Figure 13. Drug holiday resensitized DTEPs to D/T in the 3 melanoma cell lines A2058, A-375 and SK-MEL-1. For each cell lines, viability was analyzed in different conditions: parental, parental cells treated with Dabrafenib (D) and Trametinib (T) (+DT), drug-tolerant expanded persister (DTEP) cells treated with DT and DTEP cells treated with DT after drug holiday (drug hol). Treatment concentration: SK-MEL-1 (D:1mM, T: 100nM), A-375 (D:500nM, T:10nM), A2058 (D: 1mM, T:200nM). Data were normalized to day 0 (D0) and analyzed by using a one-way ANOVA on day 7. **P< 0.05, **P<0.01, ***P<0.001, ***P<0.0001, ns = non-significant*.

of the oxygen (O_2) consumption rate (OCR) of cells, in real-time, upon injection of different metabolites/inhibitors that modulate glycolysis and the mitochondrial electron transport chain (ETC). The initial injection was glucose, which is metabolized during glycolysis into pyruvate. Pyruvate can be transported into the mitochondria to fuel the Krebs cycle and the ETC. Administered second was oligomycin, a mitochondrial complex V (ATP synthase) inhibitor that blocks mitochondrial ATP synthesis, and consequently reduces OCR. The next injection was carbonylcyanide-p-trifluoromethoxyphenylhydrazone (FCCP), a potent uncoupler of mitochondrial membrane potential. FCCP induces a leakage of H+ ions across the mitochondrial membrane, allowing the ETC to operate at its maximum capacity, resulting in increased OCR. The final injection involved the simultaneous application of two inhibitors, rotenone and antimycin A, inhibiting mitochondrial complex I and III, respectively, completely blocking the ETC and decreasing OCR. As depicted in ***Figure 15***, OCR of DTEP cells, under both basal (before injections) and stressed conditions (during injections), differed from their parental counterparts in a cell line dependent manner. Specifically, SK-MEL-1 DTEP cells demonstrated similar OCR compared to parental cells, but with lower maximal OCR capacity, as evidenced by significantly lower OCR following FCCP injection (***Figure 15A***). Conversely, A-375 DTEP cells showed statistically higher mitochondrial activity in comparison to their parental counterparts, under both basal and stressed conditions (***Figure 15B***). Lastly, for the A2058 cell line, mitochondrial activity of DTEP cells was contingent upon the duration of D/T treatment. Indeed, after 20 weeks of D/T treatment A2058 DTEP cells exhibited decreased OCR compared to parental cells, during basal and stressed conditions (***Figure 15C***). Conversely, with 40 weeks of D/T treatment, the phenotype was reversed, as A2058 DTEP cells exhibited increased OCR compared to parental cells, again under both basal and stressed conditions (***Figure 15D***).Upon intricate examination of various OCR-related parameters, as illustrated in ***Figure 16A***, no significant differences were observed between parental and 20-week DTEP cells in terms of maximal-, spare- and ATP producing-OCR. In contrast, all three parameters showed a tendency to be increased in 40-week DTEP cells compared to their parental counterparts. However, this difference did not reach the significant threshold (***Figure 16B***). Indeed, these OCR-related parameters were

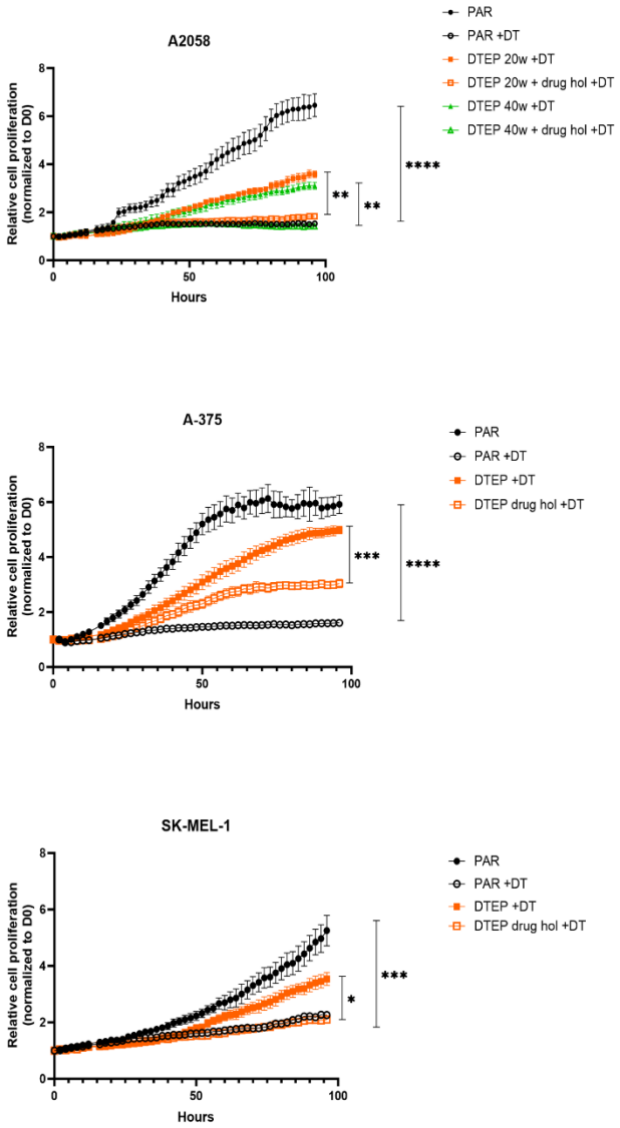

Figure 14. Drug holiday resensitized DTEPs to D/T in the 3 melanoma cell lines A2058, A-375 and SK-MEL-1. For each cell lines, proliferation were analyzed in different conditions: parental, parental cells treated with Dabrafenib (D) and Trametinib (T) (+DT), drug-tolerant expanded persister (DTEP) cells treated with DT and DTEP cells treated with DT after drug holiday (drug hol). Treatment concentration: SK-MEL-1 (D:1mM, T: 100nM), A-375 (D:500nM, T:10nM), A2058 (D: 1mM, T:200nM). Data were normalized to day 0 (DO) and analyzed by using a one-way ANOVA on hour 100. **P< 0.05, **P<0.01, ***P<0.001, ***P<0.0001, ns = non-significant*.

influenced by the variability between assays, as evidenced by the differences in OCR recorded for A2058 parental cells between experiments (***Figure 15C & D***). Taken together, melanoma DTEP cells show altered mitochondrial activity in response to D/T, that is cell line and treatment duration dependent. To further investigate metabolic alterations of melanoma DTEP cells, we selected the A2058 cell line to perform analyses of mitochondrial abundance and morphology as well as metabolic enzyme abundance, comparing between parental, 20- and 40-week DTEP cells.

4.3. A2058 DTEP cells show reduced mitochondrial abundance and a shift in mitochondrial network distribution

To assess mitochondrial abundance in A2058 parental compared to DTEP cells (D/T treated for 20- and 40-weeks), flow cytometry analysis of live cells stained with MitoTracker green was performed. This fluorescent dye rapidly and selectively labels mitochondria, allowing for precise mitochondrial quantification. In comparison to parental cells, both 20- and 40-week treated DTEP cells tended to exhibit a decrease in mitochondrial quantity, however this decrease did not reach statistical significance (***Figure 17A & B***).

After establishing a difference in mitochondrial quantity between parental and DTEP cells, confocal microscopy with MitoTracker red staining was employed to better visualize mitochondrial localization and network distribution. In parental A2058 cells, mitochondria were evenly distributed around the nucleus and exhibited symmetrical elongation of networks away from the nucleus. However, in DTEP cells treated for 20 weeks, mitochondria aggregated close to and on one side of the nucleus. Conversely, in DTEP cells treated for 40 weeks, the mitochondrial distribution resembled a transitional phenotype between parental and 20-week DTEP cells, with clusters symmetrically positioned on either side of the nucleus and similar elongated network morphology to that observed in parental cells (***Figure 17C***). Confocal microscope images were utilized to assess various parameters associated with mitochondrial distribution and morphology. The first, mitochondrial footprint, refers to the area of the image consumed

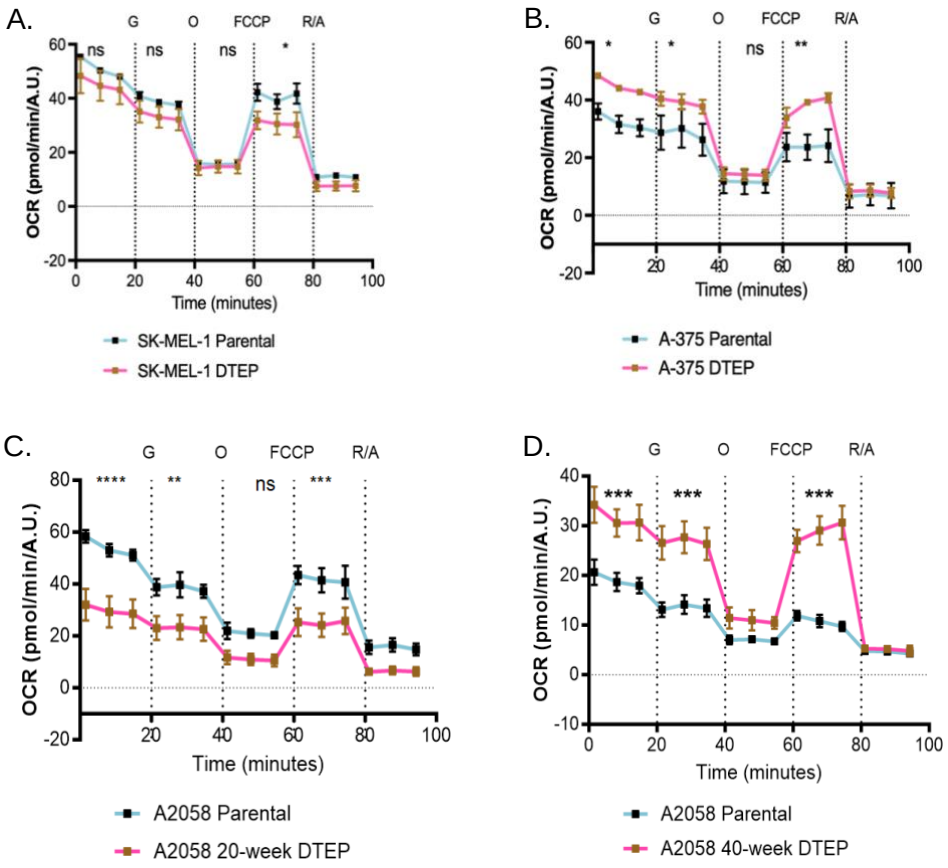

Figure 15. Oxygen consumption rates are modulated in DTEP melanoma cells in a cell line dependent manner. Kinetic measurement of oxygen consumption rate (OCR) in parental and DTEP cells of **(A)** SK-MEL-1 (n=3) **(B)** A-375 (n=3) and **(C-D)** A2058 cell lines (20-week : n=3; 40-week; n=2). OCR was measured in response to glucose (G; 100mM), oligomycin (O; 10mM), carbonyl cyanide-4 trifluoromethoxy phenylhydrazone (FCCP; 10mM), and rotenone and antimycin (R/A; 5mM, 5mM). OCR data was normalized to cell number by using Hoechst incorporation (arbitrary unit [A.U.]). One representative experiment out of three is shown and each data point represents mean ± standard error. Data were analyzed by using a two-way ANOVA followed by Bonferroni's multiple comparisons test. **P< 0.05, **P<0.01, ***P<0.001, ns = non-significant*.

by the mitochondrial signal. The second, mean branch length, represents the length of all lines used to represent mitochondrial structures. The last, mean branches network details the average number of attached lines used to represent each structure. Of these three parameters, only mitochondrial footprint showed a significant difference between parental and DTEP cells, whereby mitochondria in 20- and 40-week DTEP cells have a reduced surface area compared with parental cells (***Figure 17D***).

Similarly to observations in lung persisters, DTEP cells treated for 20 weeks exhibit decreased mitochondrial content, aligning with findings from Seahorse analysis, which demonstrated a reduction in mitochondrial activity in these cells. However, 40-week DTEPs exhibit lower mitochondrial content but higher activity compared to parental cells, suggesting that despite having fewer mitochondria, they are more active. Based on this, we decided to further investigate the mitochondrial function of these cells.

4.4. Mitochondrial complex I subunits are differentially expressed in 20- and 40-week DTEP A2058 cells

We started our investigation of mitochondrial function by assessing the expression of ETC complex subunits using quantitative PCR (gene expression) and Western blotting (protein expression). We were particularly interested in measuring the abundance of complex I subunits due to preliminary data obtained by Dr Crake in DTEP *BRAF*^{V600E} NSCLC cells, showing reduced complex I abundance compared to parental cells. Dr Crake also showed a decrease in the NAD+ to NADH ratio in DTEP cells, likely resulting from reduced complex I activity.

Due to the discrepancy between 20- and 40- week DTEP cells, we decided to also investigate earlier time points and added a timeline, including 24h to 1 week of D/T treatment on parental cells. We have compared these different time points to the 20- and 40- week DTEP cells.

Firstly, we have used a cocktail of antibodies specifically targeting a subunit in each of the ETC complexes. While no major differences were observed for complexes II, III and V, the expression of both complex I and IV subunits seemed to be slightly modulated by D/T treatment and these variations followed the same patter for

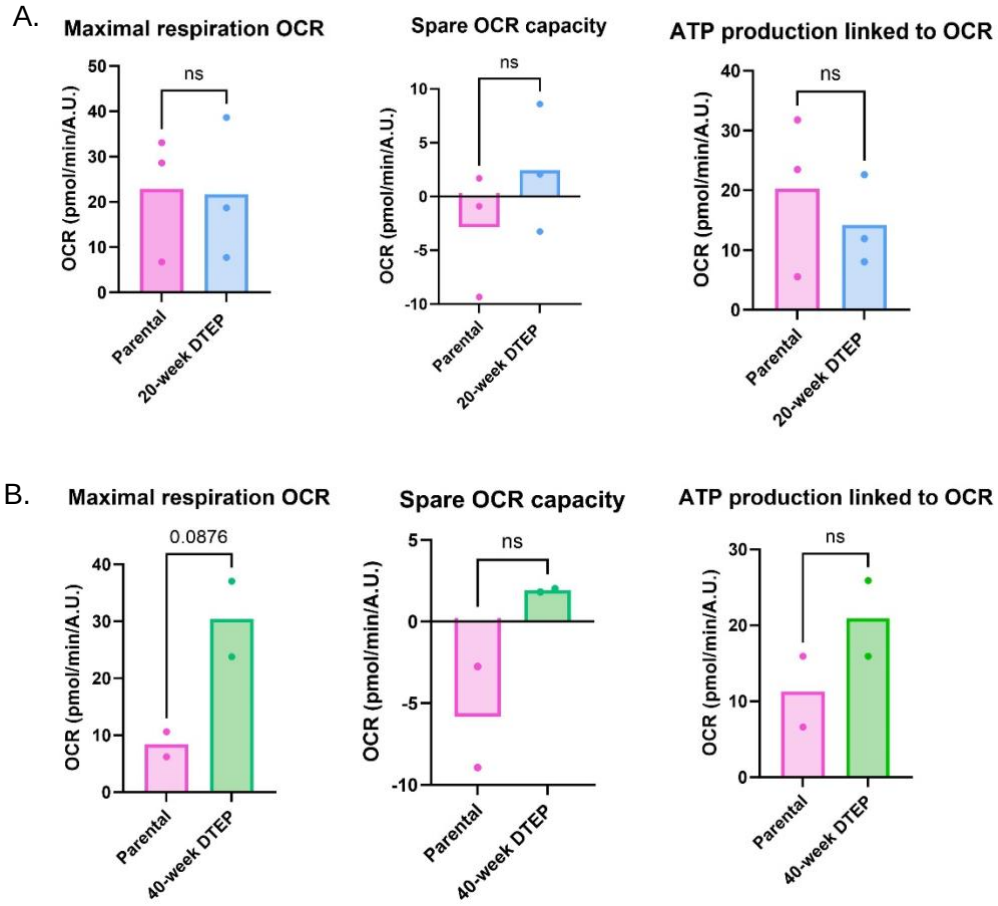

Figure 16. Oxygen consumption rates are modulated in DTEP melanoma by treatment duration. Detailed analysis of A2058 cells maximal, spare and ATP-producing OCR of parental and 20-week **(A)** and 40-week **(B)** DTEP A2058 cells, showing all biological replicates for each condition (n=3). Data were analyzed by using an unpaired t-test. **P<0.05, **P<0.01, ***P<0.001, ns = non-significant*.

both complexes ***(Figure 18A)***. The abundance of the complex I and IV subunits exhibited an increase after 72 h, and a decrease after 1 week of D/T treatment. For DTEPs, a slight increase in protein expression was observed in 20-week cells compared with parental cells, whereas for 40-week DTEP cells, it remained unchanged compared with their parental counterparts. To further confirm the results obtained with the antibody cocktail, we evaluated the expression of NDUFB8, the complex I subunit targeted by the cocktail, using another anti-NUDFB8 antibody. As depicted in ***Figure 18B***, similar results were obtained, and statistical analysis revealed that there were no significant differences in NDUFB8 protein expression between 20- and 40-week DTEP cells and their parental counterparts.

These latter results are not in good agreement with our mitochondrial network quantification (FACS analysis) and activity assay (Seahorse), described above. Indeed, the 20-week DTEPs showed reduced mitochondrial content, reduced mitochondrial activity but unchanged protein expression of the NDFUB8 subunit of complex I compared with parental cells. However, mitochondria in DTEP cells at 40 weeks were less abundant than those in parental cells, yet they have demonstrated higher activity. Nevertheless, there were no discernible differences in the protein levels of NDUFB8 or other ETC complex subunits.

Secondly, we evaluated the expression levels of genes encoding various subunits of complex I, comparing between parental and DTEP cells. We started our analysis by assessing the expression level of complex I subunits encoded by mitochondrial DNA, namely *MT-ND1*, *MT-ND2*, *MT-ND4*, and *MT-ND6* (***Figure 18C***). MT-ND is the acronym used for mitochondrially encoded NADH dehydrogenase. Overall, gene expression tended to decrease in DTEP cells, both 20- and 40-week D/T treated, however this difference was only significant for the *MT-ND1* gene in 40-week DTEP cells. Next, the expression levels of genes of complex I accessory subunits encoded by nuclear DNA were assessed, namely *NDUFA1*, *NDUFAB1*, *NDUFB1*, *NDUFB8*, and *NDUFC1*. Compared to parental cells, gene expression decreased for all the targets, except *NDUFB1,* and the downregulation was statistically significant for *NDUFA1* and *NDUFAB1* in 40-week DTEP cells *(**Figure 18C**)*. However, in 20-week DTEP cells, no

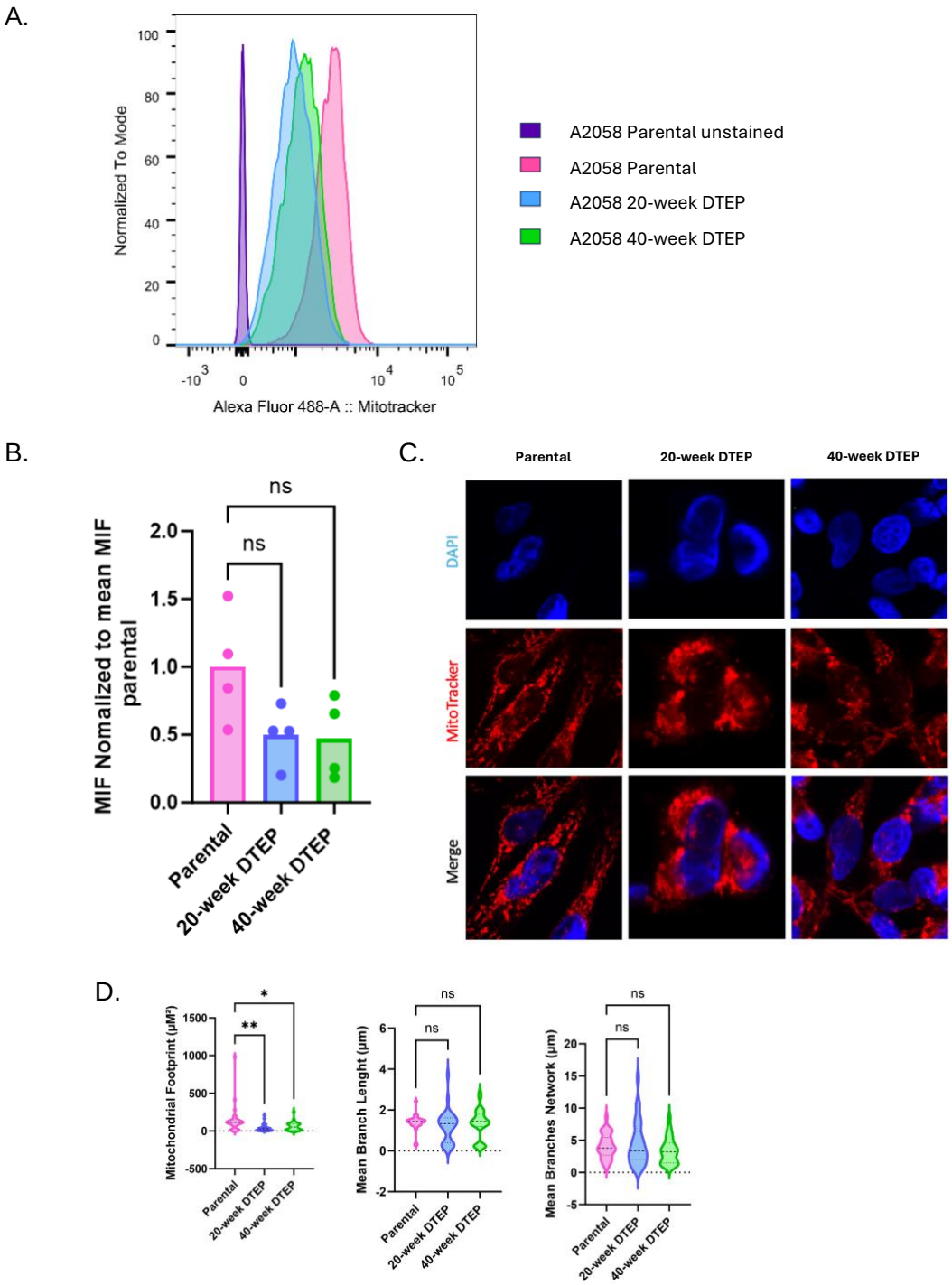

Figure 17. Drug-tolerant expanded persister (DTEP) A2058 melanoma cells demonstrate a tendency towards reduced mitochondrial abundance and a shift in mitochondrial network distribution in comparison to their parental counterparts. (A-B) Evaluation of the number of mitochondria present in parental and DTEP cells, D/T treated for 20-and 40-weeks, was performed by flow cytometry. Live cells were stained with MitoTracker conjugated to Alexa Fluor 488. An unstained condition was performed (A2058 parental unstained). For peak area, one representative experiment out of four is shown **(A)**. Median fluorescence intensity (MIF) of all biological replicates combined (n=4) is presented and statistical analysis was performed using one-way ANOVA followed by Dunnett's multiple comparisons test **(B)**. **(C)** Mitochondrial network analysis in parental and DTEP cells treated for 20- and 40- weeks using MitoTracker red staining combined with confocal microscopy. **(D)** Quantification of mitochondrial footprint, branch length and branches network in A2058 parental and 20- and 40-week cells (n=30). **P<0.05, **P<0.01, ***P<0.001, ns = non-significant*.

statistically significant differences in *NDUFA1*, *NDUFAB1*, *NDUFB1*, *NDUFB8*, and *NDUFC1* gene expression were observed when compared to parental cells.

Finally, we concluded our investigation of complex I subunits expression by examining the nuclear genes encoding core complex I subunits, *NDUFS1* and *NDUFV1*. When compared to parental cells, there was a significant reduction in mRNA expression of *NDUFS1* in 20- and 40-week DTEP cells, and *NDUFV1* in 40-week DTEP cells. Whereas, *NDUFV1* expression was comparable between parental and 20-week DTEP cells (***Figure 18C***).

Having delved into the ETC, specifically focusing on complex I, we then turned our attention to the tricarboxylic acid (TCA) cycle. It is important to note the close interconnection between the ETC and the TCA cycle. Firstly, in a cascade of enzymatic reactions, the TCA cycle produces the reducing equivalents NADH and $FADH_2$. NADH and $FADH_2$ are then shuttled to the ETC, where they donate their electrons to complexes I and II, respectively, to initiate the flow of electrons along the chain and drive the production of ATP though oxidative phosphorylation. Secondly, succinate dehydrogenase (SDH) is a key enzyme in both the TCA cycle and the ETC. Indeed, in the TCA cycle, SDH catalyzes the oxidation of succinate to fumarate, by reducing FAD to $FADH_2$. In the ETC, SDH represents complex II, which facilitates the transfer of electrons to coenzyme Q, thus, contributing to the generation of a proton gradient across the inner mitochondrial membrane and ATP production. The SDH enzyme is composed of 4 subunits: SDHA and SDHB represent the catalytic subunits, while SDHC and SDHD provide membrane anchorage. As shown in ***Figure 19,*** the expression of SDHA was stable in parental and DTEP cells both at the protein (***Figure 19A***) and the mRNA (***Figure 19B***) levels.

4.1. Expression of TCA cycle enzymes remained unchanged in DTEP A2058 cells

In addition to SDH complex, we investigated key TCA cycle enzymes (***Figure 20A***). We started by analyzing the abundance of pyruvate dehydrogenase (PDH), enabling the

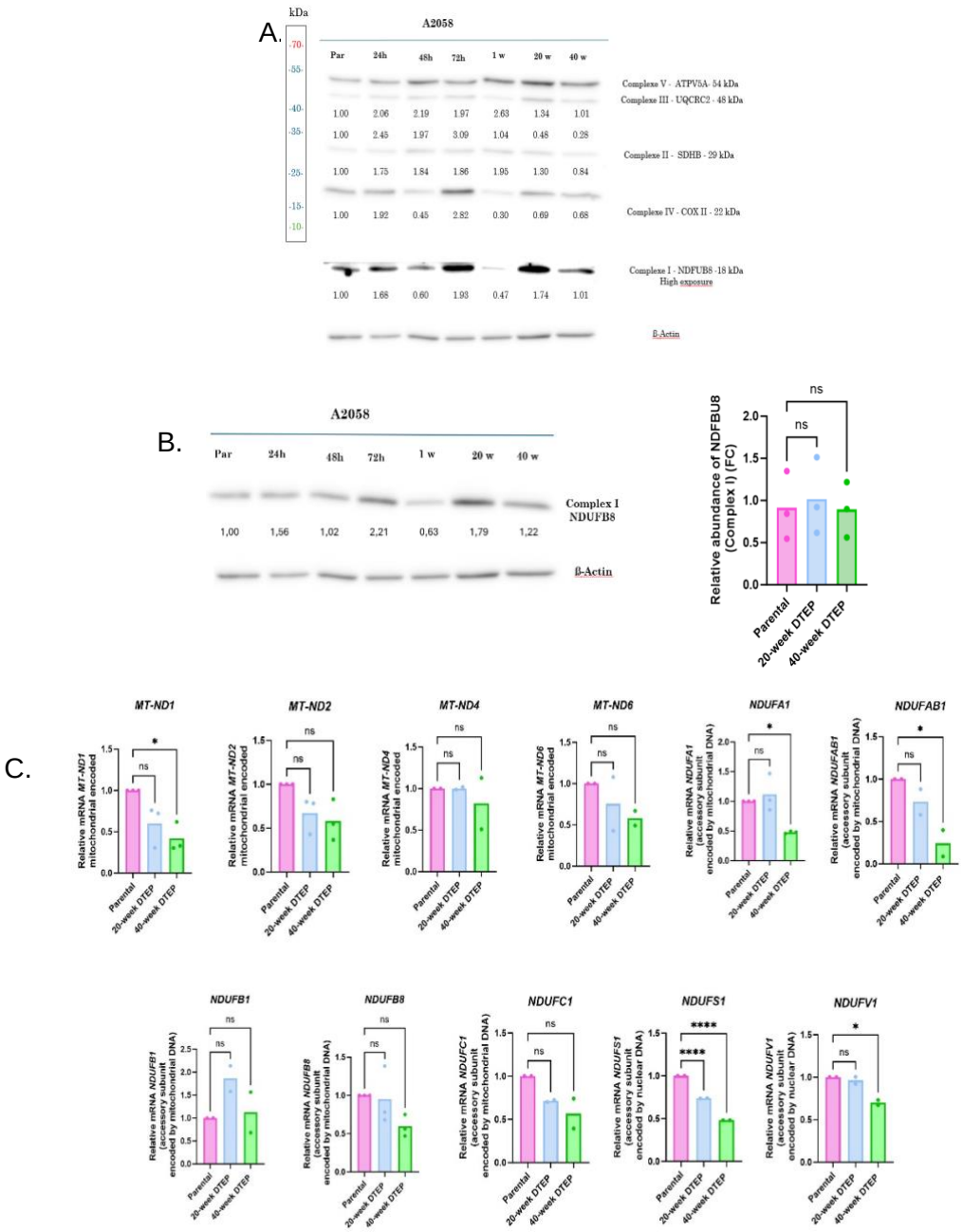

Figure 18. A2058 drug-tolerant expanded persister (DTEP) cells demonstrate varying expression levels of mitochondrial complex I subunits. (A) Western blot analysis of mitochondrial ETC complex subunits (one subunit per complex I-V): ATPV5A from complex V, UQCR2 from complex III, SDHB from complex II, COX II from complex IV and NDUFB8 from complex I. Mitochondrial ETC complex subunit expression was measured in A2058 cells in response to Dabrafenib and Trametinib over time (n=1). **(B)** Western blot analysis of NDUFB8 (complex I subunit) in A2058 cells in response to Dabrafenib and Trametinib over time. β-actin was used as a loading control for all Western blots (24h-1w: n=1; 20w-40w: n=3). **(C)** Relative mRNA levels of mitochondrial complex I subunits encoded by mitochondrial DNA: mitochondrially encoded NADH dehydrogenase 1 *(MT-ND1*), mitochondrially encoded NADH dehydrogenase 2 (*MT-ND2*), mitochondrially encoded NADH dehydrogenase 4 (*MT-ND4*), mitochondrially encoded NADH dehydrogenase 6 (*MT-ND6*); of mitochondrial complex I accessory subunits encoded by nuclear DNA: *NDUFA1, NDUFAB1, NDUFB1, NDUFB8*, and *NDUFC1 and* core subunits encoded by nuclear DNA: *NDUFS1* and *NDUFV1*. Data were analyzed by using a one-way ANOVA followed by Dunnett's multiple comparison test. Each dot present one experiment (n=2 or n=3).**P< 0.05, **P<0.01, ***P<0.001, ****P<0.0001, ns = non-significant*

conversion of pyruvate into acetyl-CoA. The western blot analysis revealed that PDH expression remained unaffected in 40-week DTEP cells (***Figure 20B***).

We also assessed the PDH inactivation status by examining its phosphorylated (pPDH Ser293) form and once again, there were no discernible differences between parental and 40-week DTEP cells (***Figure 20B***). A slight decrease of the expression of both isocitrate dehydrogenase 1 (IDH1) and fumarase, which facilitate the conversion of isocitric acid into α-ketoglutaric acid and fumarate to malate, respectively, was observed in 40-week DTEP cells (***Figure 20C***).

4.2. DTEP A2058 cells have reduced expression of glycolysis-associated enzymes

To further explore potential differences in energetic metabolism between parental cells and DTEPs, we next examined abundance of glycolysis enzymes. Glycolysis is a crucial metabolic pathway occurring in the cytoplasm that breaks down glucose to generate pyruvate. Subsequently, pyruvate is converted into acetyl-CoA, which enters the mitochondrial matrix or into lactate. Within the matrix, acetyl-CoA undergoes oxidation in the TCA cycle, generating NADH and $FADH_2$. These electron carriers then participate in the electron transport chain, ultimately leading to the production of ATP.

To study glycolysis, quantitative real-time PCR (RT-qPCR) and western blot analysis were performed to assess the expression of different genes coding for transporters and enzymes involved in glycolysis and lactate metabolism. Since glycolysis begins by glucose entering the cell, we analyzed the mRNA expression of the class 1 glucose transporter, GLUT1. Compared to parental cells, GLUT1 expression is significantly decreased in 20- and 40-week DTEP cells. (***Figure 21B***). The reduction of GLUT1 expression in DTEPs was further confirmed through western blot analysis, as depicted in ***Figure 21C***.

The first step of the glycolytic pathway involves the conversion of glucose to glucose-6-phosphate, by hexokinase 2 (HK2). Western blot analysis demonstrated that HK2 expression remains consistent between parental and 40-week DTEP cells (***Figure 21C***).

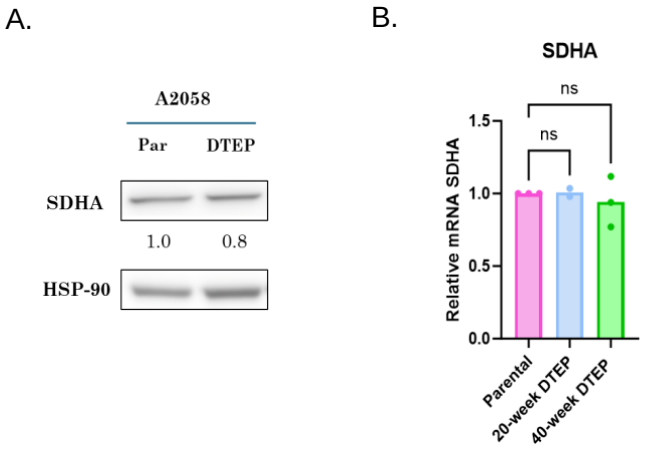

Figure 19. The expression of succinate dehydrogenase A in A2058 drug-tolerant expanded persister (DTEP) cells remains unaltered when compared to parental cells. (A) Western blot analysis of succinate dehydrogenase A (SDHA) measured in A2058 parental and 40-week DTEP cells (n=1). HSP90 was used as a loading control for all Western blots. **(B)** Relative mRNA levels of SDHA in A2058 parental and 20- and 40-week DTEP cells. Data were analyzed by using a one-way ANOVA followed by Dunnett's multiple comparison test. Each dot represent one experiment (n=3). *ns= non-significant*.

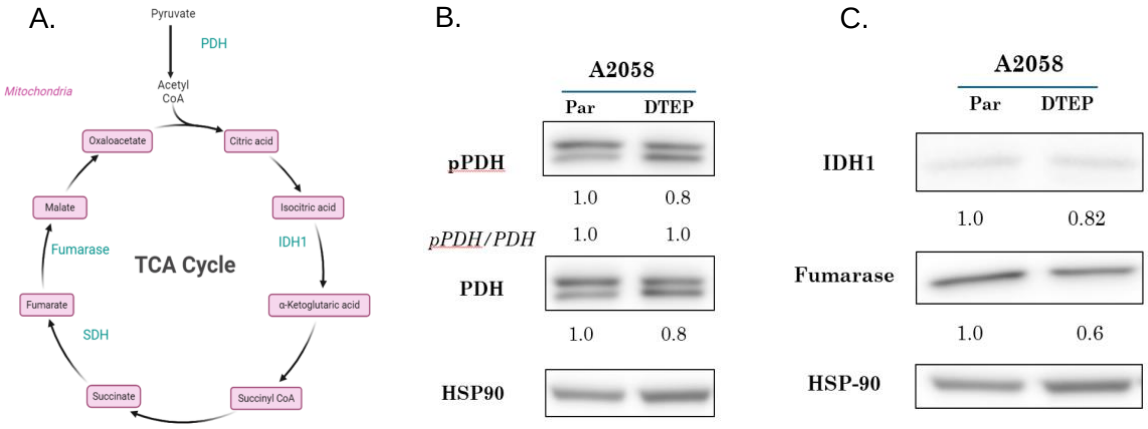

Figure 20. Drug-tolerant expanded persister (DTEP) A2058 melanoma cells exhibit unchanged expression of TCA cycle enzymes. (A) Schematic illustrating tricarboxylic acid (TCA) cycle. Western blot analysis of pyruvate dehydrogenase (PDH) and its phosphorylated form (pPDH Ser293) **(B)**, isocitrate dehydrogenase 1 (IDH1) and fumarase **(C)** in A2058 parental and 40-week DTEP cells (n=1). HSP90 was used as a loading control for all Western blots.

We further investigated the mRNA expression of another key enzyme, phosphoglycerate kinase 1 (PGK1), which converts 1,3-bis phosphoglycerate into 3-phosphoglycerate. RT-qPCR analysis showed no change in *PGK1* mRNA levels between parental and both 20- and 40-week DTEP cells (***Figure 21B***). At the end of glycolysis, pyruvate generated in the cytoplasm can enter the mitochondria through a transporter known as mitochondrial pyruvate carrier 2 (MPC2). Western blot analysis of MPC2 protein expression level indicated no difference between parental and 40-week DTEP cells (***Figure 21C***).

Finally, we investigated the expression of additional pivotal players in lactate metabolism, such as lactate dehydrogenase A (LDHA) and monocarboxylate transporters 1 and 4 (MCT1 and MCT4). LDHA catalyzes the conversion of pyruvate to lactate, and MCT1 and MCT4 are responsible for facilitating lactate transportation into and out of the cell, respectively. qPCR results revealed that expression levels of *LDHA*, *MCT1* and *MCT4* were significantly lower in 20- and 40-week DTEP compared to parental cells (***Figure 21B***).

These findings collectively indicated a substantial reduction in the expression of some genes associated with glycolysis in DTEP cells, when compared to their parental counterparts.

4.3. Statins did not affect the viability of DTEP melanoma cells

The final objective of my work was to evaluate whether DTEP A2058 cell viability is differentially impacted by statins. As previously shown, Dr Crake observed that NSCLC DTEP cells were sensitive to statins by decreasing their viability and ability to form colonies. Hence, we aimed to determine whether similar observations could be made in melanoma DTEP cells. Statins are inhibitors of the mevalonate pathway which, beside the production of cholesterol, plays a crucial role in the synthesis of coenzyme Q10, an essential electron carrier within the ETC. Indeed, statins block the conversion of HMG-CoA to mevalonate, thereby reducing the production of coenzyme Q10 downstream of mevalonate. Due to the decreased and increased OCR observed in 20-week and 40-week DTEP cells, respectively, we hypothesized that 40-week DTEP cells would be more sensitive to statins, due to their heightened reliance on ETC activity.

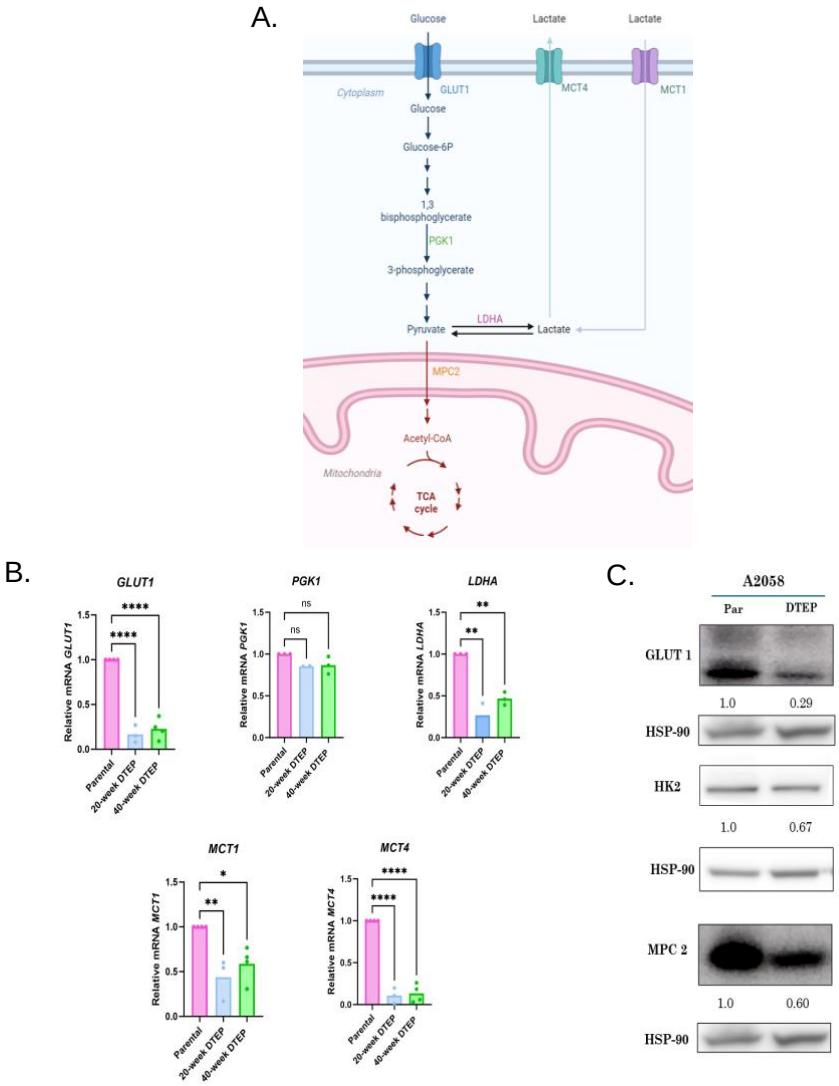

Figure 21. Drug-tolerant expanded persister (DTEP) A2058 melanoma cells exhibit a propensity for decreased expression of enzymes involved in glycolysis . (A) Schematic illustrating glycolysis and lactate metabolism. **(B)** Relative mRNA levels of Class 1 glucose transporter (GLUT1), phosphoglycerate kinase 1 (PGK1), lactate dehydrogenase A (LDHA), monocarboxylate transporter 1 (MCT1) and 4 (MCT4) in A2058 parental cells, drug-tolerant expanded persister (DTEP) cells treated for 20 weeks and 40 weeks. Data were analyzed by using a one-way ANOVA followed by Dunnett's multiple comparison test. Each dot represents one experiment (n=3). **(C)** Western blot analysis of GLUT1, hexokinase 2 (HK2) and mitochondrial pyruvate carrier 2 (MPC2) in A2058 parental and 40-week DTEP cells (n=1). HSP90 was used as a loading control for all Western blots. **P< 0.05, **P<0.01, ***P<0.001, ****P<0.0001, ns= non-significant*

However, based on half-maximal inhibitory concentration (IC50) analysis of fluvastatin, there was no difference in cell viability between parental (IC50= 3.3μM) and 20- (IC50= 2.2μM) and 40-week (IC50=1.83μM) DTEP cells (***Figure 22B***).

We also aimed to investigate the expression levels of enzymes closely or remotely involved in the mevalonate pathway. We initiated this study by examining the protein levels of ATP citrate lyase (ACLY) as well as its activation level (pACLY Ser455). This enzyme converts citric acid, produced by the TCA cycle, into acetyl-CoA, in order to fuel biochemical reactions involved in the synthesis of fatty acids and cholesterol. Therefore, ACLY acts directly upstream of the mevalonate pathway. Our analysis revealed a slight decrease in the expression and activation of ACLY in 40-week DTEP cells compared to parental counterparts (***Figure 22C***). However, mRNA levels of HMG-CoA reductase (HMGCR), another key enzyme of the mevalonate pathway capable of converting HMG-CoA into mevalonate, were stable in DTEP cells (***Figure 22D***).

Conversely to what has been observed by Dr. Crake, these results suggest that DTEP cells, either 20-week and 40-week, are not dependent on the mevalonate pathway.

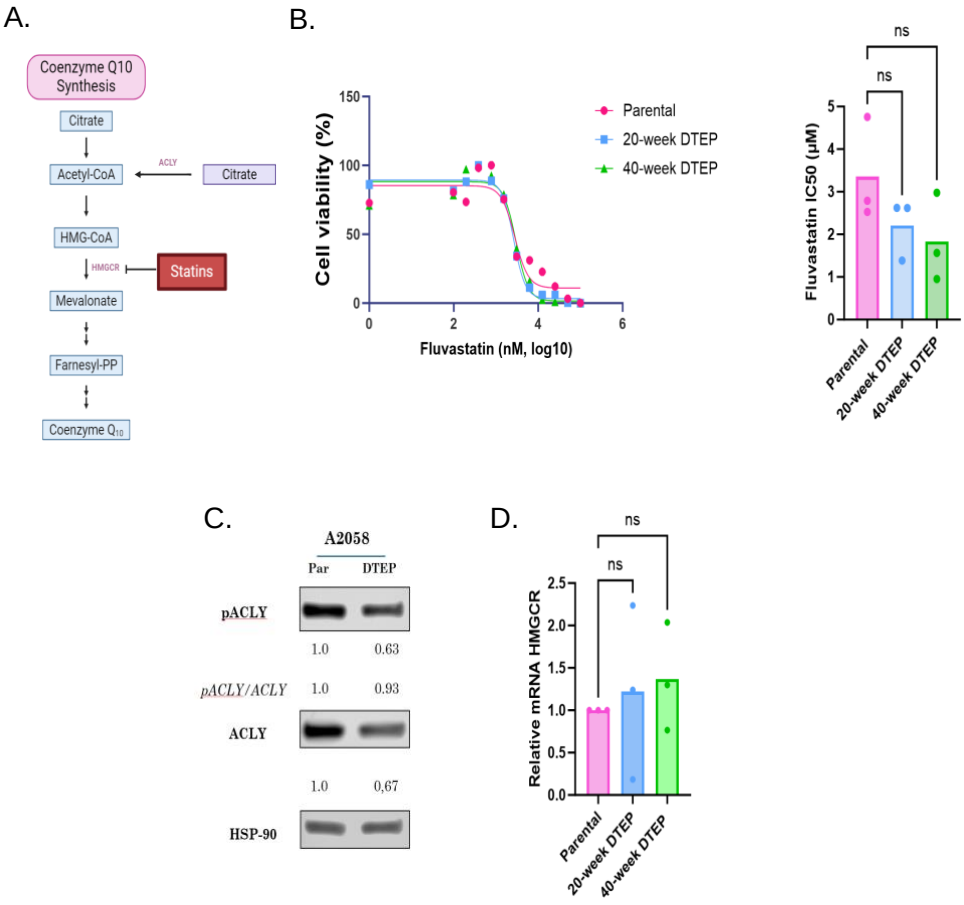

Figure 22. Fluvastatin impacts cell viability of A2058 parental and drug-tolerant expanded persister (DTEP) cells in similar manner. (A) Schematic illustrating mevalonate pathway. **(B)** Half-maximal inhibitory concentration (IC50) analysis of Fluvastatin on A2058 parental and 20- and 40-week DTEP cells (n=3). One representative experiment is depicted for IC50 curves. **(C)** Western blot analysis of ATP citrate lyase (ACLY) and its phosphorylated form (pACLY Ser455) in A2058 parental and 40-week DTEP cells (n=1). HSP-90 was used as a loading control. **(D)** Relative mRNA levels of HMG-CoA reductase (HMGCR) in A2058 parental cells, drug-tolerant expanded persister (DTEP) cells treated for 20 weeks and 40 weeks. Data were analyzed by using a one-way ANOVA followed by Dunnett's multiple comparison test. Each dot represents one experiment (n=3). *ns = non-significant*

5. Discussion

Cancers with the *BRAF*^{V600E} mutation, such as melanoma or non-small cell lung cancer (NSCLC), are aggressive cancers that develop due to hyperactivation of the MAPK pathway, leading to uncontrolled cell proliferation. This mutation drives the excessive growth and survival of cancer cells, making these cancers particularly challenging to treat. Among the therapeutic options available, targeted therapy is proving to be an asset in the treatment of *BRAF*^{V600E} mutated cancers. Dabrafenib, in particular, specifically targets the mutated form of BRAF, inhibits its activity and thereby reduces the hyperactivation of the MAPK pathway. In addition, various clinical studies (NCT01336634, NCT01682083) have shown that, compared to BRAF inhibitor monotherapy, combining BRAF inhibitors with another MAPK pathway inhibitor, such as the MEK inhibitor (Trametinib), significantly enhances the tumor response to treatment[55,87]. Even though this D/T combination can improve response and slow the development of treatment resistance, some cells inevitably develop resistant. Drug-tolerant expanded persister (DTEP) cells are considered as the reservoir from which resistant cells eventually emerge. Evidence suggests that while becoming persistent, DTEP cells adapt their energetic metabolism. It was recently shown that DTEP melanoma cells exhibit improved mitochondrial function[88]. Interestingly, our laboratory has found that NSCLC DTEP cells, tolerant to D/T, behave oppositely to melanoma DTEP cells, displaying decreased mitochondrial activity. The objective of my master thesis was therefore, to evaluate the metabolic adaptations of melanoma DTEP cells generated through the same protocol than the one followed for lung DTEP. To achieve this objective, before my arrival in the laboratory, DTEP cells were obtained by treating three melanoma cell lines, A2058, A-375, and SK-MEL-1, with Dabrafenib and Trametinib for 20 and 40 weeks.

During the course of this work, we were able to:

1) Show that melanoma D/T persister cells exhibited altered mitochondrial morphology and activity compared to their parental counterparts.
2) Observe a huge discrepancy in term of oxygen consumption rates (OCR) between the different cell lines analyzed.

3) Demonstrate that some TCA and glycolytic enzymes are downregulated in DTEP cells.
4) Highlight that DTEP melanoma cells do not rely on the mevalonate pathway for their survival, as they show similar sensitivity to statins than parental cells.

Overall the objectives of my master thesis were fulfilled. However, our results obtained in the context of melanoma, showed some discrepancies with the existing literature, as well as with preliminary data from our laboratory investigating lung persister models. The current findings, therefore, shed light on some limitations of our models and raise novel questions. Discussed below are the main results, the limitations and the perspectives of this study.

Given that drug tolerance is characterized by a transitory and reversible phenotype, restoring the sensitivity of cells to the drugs can be accomplished by a "drug washout" or "drug holiday". We therefore assessed the impact of a drug holiday on the viability and proliferation of melanoma cells, using MTT and Incucyte assays, respectively. While the MTT assay is considered as a viability test based on mitochondrial activity, the follow-up of cell numbers in real time with the Incucyte allow a quantification of cell proliferation[89]. Overall, the results obtained with the two techniques are comparable and the curves follow the same trend. Specifically, for A-375 cells, the growth of DTEP cells after the drug holiday was significantly lower than the DTEP cells maintained with D/T, as shown with the Incucyte results. However, this difference was much less obvious with the MTT assay. In this case and due to the alteration of mitochondria in DTEP cells, the MTT assay might be less reliable to evaluate cell growth compared to cell number quantification[89]. However, the MTT assay is still widely used in our laboratory for a quick and low-cost assessment of cell viability. On the other side, the MTT assay provides a punctual measure of cell viability at selected time points. While the Incucyte assay offers continuous and detailed monitoring of cell proliferation. We therefore concluded that the Incucyte assay should be used to validate the results obtained by MTT assay as a first step. Interestingly, the literature regarding studies of persister phenotypes, is growing exponentially in the field of melanoma. Further works are also needed to establish a common definition of persister cells and achieve a consensus among the

scientific community to determine the specific characteristics and markers of these populations in preclinical models.

As mentioned above, my first objective was to evaluate mitochondrial morphology and activity in BRAF mutant persister cells. To study mitochondrial biogenesis, three key parameters need to be considered: the presence of reactive oxygen species (ROS), mitochondrial mass and mtDNA content[90, 91]. In this work, we focused on the two latter aspects. Firstly, we observed that D/T persister BRAF mutant melanoma cells exhibited a reduced mitochondrial content compared to parental cells. These results contradict those published by the group of Corazao-Rozas *et al*., who demonstrated a significant increase in mitochondrial mass, as evidenced by the increase of mitochondrial DNA content following exposure to Vemurafenib (BRAF inhibitor)[77]. To validate our results obtained by FACS and imaging, we could assess mitochondrial contents in DTEP cells using specific primers for nuclear and mitochondrial genes by qPCR.

In addition to mitochondrial abundance, a functional analysis of oxygen consumption rates (OCR) by melanoma DTEP cells was conducted using the Seahorse XF analyzer. Of note, inconsistent results were obtained between the different cell lines evaluated, and within the same cell line, with the different duration of treatment (e.g. A2058 and their DTEPs treated with D/T for 20 or 40 weeks). When considering the results obtained for the A-375 DTEP cells and the A2058 40-week DTEP cells, they are consistent with those reported by the literature. Indeed, Shen *et al*. also reported higher OCR, and thus, increased mitochondrial activity in A-375 DTEP compared to parental cells, which were established from treatment with Vemurafenib (BRAFi) and Combimetinib (MEKi)[80]. Surprisingly, when examining the A2058 40-week DTEP cells, they exhibit increased mitochondrial function compared to parental cells despite having a reduced number of mitochondria. In line with reduced mitochondrial numbers, 40-week DTEP A2058 cells also show a decrease in the expression of complex I subunit and TCA cycle genes. It is possible to infer that even though these mitochondria are fewer in number, they function more efficiently, allowing the A2058 40-week DTEP cells to have superior mitochondrial activity compared to parental cells. Furthermore, the expression of key glycolysis-related enzymes/transporters, such as GLUT1, HK2, MCT1, MCT4 and LDHA, are notably

decreased in 40-week DTEP A2058 cells. These results are in good agreement with the study of Shen *et al*., associating the increased oxidative phosphorylation with a reduction of glycolysis in DTEP cells[80]. In contrast, the results obtained for DTEP SK-MEL-1 cells, and 20-week DTEP A2058 cells do not align with the existing literature on melanoma, as these DTEPs exhibited lower mitochondrial activity compared to their parental cells in our study, which correlates more closely with our findings for DTEP cells derived from NSCLC[77,90]. These results highlight some heterogeneity between our different models, suggesting the presence of potential co-mutations along with $BRAF^{V600E}$, and highlighting the need of a deeper characterization of the basal energetic metabolism and nutrient dependency of each cell line. Another limitation that should also be considered is the high variability observed in parental A2058 cells, when comparing between experiments performed with the 20- and 40-week DTEPs, such as in the OCR analysis. However, we know that direct comparison between different Seahorse experiments is difficult due to many technical factors (such as, calibration, temperature, small variations in medium preparation,...). An additional experiment directly comparing OCR between 20- and 40-week DTEPs, should help clarify any differences in the mitochondrial activity of these cells. In $BRAF^{V600E}$ NSCLC persisters, Dr. Crake observed that decreased mitochondrial activity is correlated with a downregulation of some ETC complex I subunits. Based on the current studies OCR results, our hypothesis was that the expression of complex I subunits should be lower and higher in 20- and 40-week DTEP, respectively, when compared to their parental counterparts. While no major differences were observed in 20-week DTEPs, the gene expression of *NDUFB8* was decreased in 40-week DTEP compared to parental cells. At the protein level, the abundance of NDUFB8 was similar between 40-week DTEP and parental cells. These disparities could be partially explained by a higher stability of the protein in a persister context, or by the findings from Dr. Robert's team, which reported a reversible remodeling of the translation of certain mRNAs in a subpopulation of $BRAF^{V600E}$ mutant melanoma cells that tolerate exposure to BRAF and MEK inhibitors[92]. Although tolerance was associated with an overall decrease in protein synthesis, certain mRNAs exhibit an increased expression. Therefore, despite its decreased gene expression, the translation efficiency of *NDUFB8* mRNA to protein could be increased resulting in protein expression levels similar to those of the parental cells[92].

In parallel to our observations related to NDUFB8 expression, we noticed decreased mRNA levels of several complex I subunits such as *MT-ND1*, *NDUFS1* and *NDUFAB1*. Thus, the protein levels of these other components should also be evaluated, in order to further confirm the potential implication of complex I in the persister phenotype. Interestingly, we demonstrated a reduction in mitochondrial quantity in DTEP cells which could lead to a lower mtDNA content per cell and in turn could result in diminished expression of mtDNA encoded subunits. We could, therefore, focus our attention on these subunits first, but without excluding the potential epigenetic, genetic or transcriptional regulation of nuclear DNA encoded subunits.

In addition, the decreased abundance of some key TCA cycle enzymes in 40-week A2058 DTEPs, is not in agreement with the increased OCR observed in these cells, or with the existing literature on melanoma persister cells. Indeed, Karki *et al*. demonstrated a transient upregulation in TCA cycle metabolism in melanoma persister cells, showing a higher consumption rate of TCA cycle metabolites than in parental cells[93]. In the future, the expression of the other TCA cycle enzymes should be evaluated. Secondly, and more importantly, the activity of these enzymes should be assessed to confirm the potential reduced TCA cycle flux. Indeed, Shen *et al*. reported an increased TCA cycle flux in DTEPs compared to parental cells in melanoma persister cells[80]. Similarly to our preliminary results obtained in lung D/T persisters, the ratio NAD+/NADH could be determined as a readout of TCA cycle activity.

Based on our preliminary results, the glycolytic rate is also decreased in A2058 DTEPs. It has also been reported by Corazao-Rozas *et al*. that glycolysis is decreased in melanoma cells treated with targeted therapy, favoring oxidative phosphorylation[77]. Therefore, additional readouts of glucose uptake and lactate production should also be performed, in order to complete our understanding. Altogether, in 20-week A2058 persisters, both glycolysis and mitochondrial respiration are downregulated. These results could be associated with the reduced proliferation rate of these cells compared to parental A2058 cells. Decreased expression of glycolysis enzymes and mitochondrial respiration are not in agreement with the existing literature, but partially confirmed the results obtained by Dr. Crake in BRAF mutant lung persisters.

Conversely, in the long term persisters (40-week), the interpretation of the results is more complex. While the expression of both glycolysis and TCA cycle enzymes are decreased, the OCR is increased in these cells despite a lower mitochondrial content. As mentioned above, we have some doubts regarding the Seahorse results. Therefore, additional controls should be performed for the Seahorse assay, and these should be combined with further investigations of ATP production and mitochondrial membrane potential (using TMRE probe) measurements in both 20- and 40-week DTEPs. In case we confirm the increased OCR in 40-week persister cells, we would next evaluate the metabolic dependency of these cells to other metabolites, such as glutamine and fatty acids, using specific medium deprivation or inhibitors of these catabolic pathways.

Our final objective was to determine vulnerabilities acquired in persister cells. Unfortunately, in contrast with what has been observed with lung cancer persister cells, melanoma persister cells are not sensitive to statins. Dr. Crake correlates the increased sensitivity to statins of lung persisters to the decreased expression of complex I subunits and an increased dependency of coenzyme Q10 to fuel the ETC. Interestingly, the dependency of lung persister cells to protein prenylation and N-glycosylation, two other downstream targets of the mevalonate pathway, are currently under investigation in the Laboratory. Given that mitochondrial metabolism is increased in melanoma DTEP cells, it has been shown that directly targeting the mitochondria can effectively kill these DTEP cells. Indeed, Hong *et al*. demonstrated that using antioxidant agents coupled with a lipophilic cation, which allows their accumulation in the mitochondria, can disrupt mitochondrial bioenergetics in human *BRAF*^{V600E} melanoma cell lines[94]. This strategy could thus be tested on 40-week DTEP A2058 cells, potentially offering a novel therapeutic approach to eliminate these persistent melanoma cells.

6. Conclusion and perspectives

My first goal, aiming at validating the persister/tolerant phenotype of our *BRAF*^{V600E} melanoma DTEP cells, was successfully achieved. After, in order to better understand the discrepancy between the results obtained by Dr. Crake in a lung context and the existing literature in melanoma, my second objective was to characterize the metabolic adaptations associated to the transient tolerant state to target therapy in *BRAF*^{V600E} melanoma cells. We used a validated model of "drug-tolerant persister" cells obtained by treating different melanoma cell lines with D/T for several weeks. Our results highlighted a lineage-dependent metabolic activity in melanoma DTEP cells, with an increased mitochondrial respiration in 40-week DTEP A2058 and A-375 cells, following patterns previously shown in the literature. Further characterization showed a reduced expression of key players involved in both glycolytic and mitochondrial metabolism/content. These potential discrepancies highlight the need for further analysis to better evaluate the activity of both glycolytic and mitochondrial respiration pathways, in addition to the expression levels of key actors in these pathways. The third objective was to evaluate the sensitivity of melanoma DTEPs to statins, inhibitors of the mevalonate pathway. According to the results obtained in the lung persister context, our hypothesis was that DTEPs with altered mitochondrial function should suffer from statin-mediated inhibition of coenzyme Q10 production. We demonstrated that both DTEP A2058 cells and parental cells show similar sensitivity to statins treatment. Therefore, it is likely that differential therapeutic strategies should be implemented in order to specifically target D/T DTEP cells in the lung and melanoma contexts. The next step will be to decipher the potential metabolic dependencies of these cells by metabolite deprivation and metabolic pathway pharmacologic inhibition. In parallel, we will perform the same evaluation of glycolysis, TCA cycle and ETC players expression and activity in DTEPs obtained from other cell lines.

Overall, the data obtained do not allow us to draw definitive conclusions about the metabolic adaptations employed by melanoma cells under sustained D/T treatment pressure. Further investigations are necessary to elucidate how *BRAF*^{V600E} mutated cancer cells adapt their metabolic phenotypes upon D/T treatment, to identify a novel line of treatment after first-line targeted therapy.

7. Bibliography

1. Guo, Y. *et al.* ERK/MAPK signalling pathway and tumorigenesis (Review). *Exp Ther Med* (2020) doi:10.3892/etm.2020.8454.
2. Jeffrey, K. L., Camps, M., Rommel, C. & Mackay, C. R. Targeting dual-specificity phosphatases: manipulating MAP kinase signalling and immune responses. *Nat Rev Drug Discov* **6**, 391–403 (2007).
3. Raman, M., Chen, W. & Cobb, M. H. Differential regulation and properties of MAPKs. *Oncogene* **26**, 3100–3112 (2007).
4. Katz, M., Amit, I. & Yarden, Y. Regulation of MAPKs by growth factors and receptor tyrosine kinases. *Biochimica et Biophysica Acta (BBA) - Molecular Cell Research* **1773**, 1161–1176 (2007).
5. Lowenstein, E. J. *et al.* The SH2 and SH3 domain-containing protein GRB2 links receptor tyrosine kinases to ras signaling. *Cell* **70**, 431–442 (1992).
6. Simon, J. A. & Schreiber, S. L. Grb2 SH3 binding to peptides from Sos: evaluation of a general model for SH3-ligand interactions. *Chem Biol* **2**, 53–60 (1995).
7. Wellbrock, C., Karasarides, M. & Marais, R. The RAF proteins take centre stage. *Nat Rev Mol Cell Biol* **5**, 875–885 (2004).
8. Dankner, M., Rose, A. A. N., Rajkumar, S., Siegel, P. M. & Watson, I. R. Classifying BRAF alterations in cancer: new rational therapeutic strategies for actionable mutations. *Oncogene* **37**, 3183–3199 (2018).
9. Roskoski, R. RAF protein-serine/threonine kinases: Structure and regulation. *Biochemical and Biophysical Research Communications* **399**, 313–317 (2010).
10. Macdonald, S. G. *et al.* Reconstitution of the Raf-1-MEK-ERK signal transduction pathway in vitro. *Mol Cell Biol* **13**, 6615–6620 (1993).
11. Zheng, C. F. & Guan, K. L. Cloning and characterization of two distinct human extracellular signal-regulated kinase activator kinases, MEK1 and MEK2. *Journal of Biological Chemistry* **268**, 11435–11439 (1993).
12. Papin, C. *et al.* B-Raf protein isoforms interact with and phosphorylate Mek-1 on serine residues 218 and 222. *Oncogene* **10**, 1647–1651 (1995).
13. Mebratu, Y. & Tesfaigzi, Y. How ERK1/2 Activation Controls Cell Proliferation and Cell Death Is Subcellular Localization the Answer? *Cell Cycle* **8**, 1168–1175 (2009).
14. Meloche, S. & Pouysségur, J. The ERK1/2 mitogen-activated protein kinase pathway as a master regulator of the G1- to S-phase transition. *Oncogene* **26**, 3227–3239 (2007).

15. Dhillon, A. S., Hagan, S., Rath, O. & Kolch, W. MAP kinase signalling pathways in cancer. *Oncogene* **26**, 3279–3290 (2007).
16. Sinkala, M., Nkhoma, P., Mulder, N. & Martin, D. P. Integrated molecular characterisation of the MAPK pathways in human cancers reveals pharmacologically vulnerable mutations and gene dependencies. *Commun Biol* **4**, 1–16 (2021).
17. Holderfield, M., Deuker, M. M., McCormick, F. & McMahon, M. Targeting RAF kinases for cancer therapy: BRAF-mutated melanoma and beyond. *Nat Rev Cancer* **14**, 455–467 (2014).
18. Davies, H. *et al.* Mutations of the BRAF gene in human cancer. *Nature* **417**, 949–954 (2002).
19. Wan, P. T. C. *et al.* Mechanism of Activation of the RAF-ERK Signaling Pathway by Oncogenic Mutations of B-RAF. *Cell* **116**, 855–867 (2004).
20. Zhang, B.-H. & Guan, K.-L. Activation of B-Raf kinase requires phosphorylation of the conserved residues Thr598 and Ser601. *EMBO J* **19**, 5429–5439 (2000).
21. Enumah, S. *et al.* BRAFV600E Mutation is Associated with an Increased Risk of Papillary Thyroid Cancer Recurrence. *World J Surg* **44**, 2685–2691 (2020).
22. Grothey, A., Fakih, M. & Tabernero, J. Management of BRAF-mutant metastatic colorectal cancer: a review of treatment options and evidence-based guidelines. *Annals of Oncology* **32**, 959–967 (2021).
23. Wang, R. *et al.* Analysis of major known driver mutations and prognosis in resected adenosquamous lung carcinomas. *J Thorac Oncol* **9**, 760–768 (2014).
24. Rosell, R. & Karachaliou, N. Large-scale screening for somatic mutations in lung cancer. *Lancet* **387**, 1354–1356 (2016).
25. Nokin, M.-J., Ambrogio, C., Nadal, E. & Santamaria, D. Targeting Infrequent Driver Alterations in Non-Small Cell Lung Cancer. *Trends Cancer* **7**, 410–429 (2021).
26. Bray, F. *et al.* Global cancer statistics 2022: GLOBOCAN estimates of incidence and mortality worldwide for 36 cancers in 185 countries. *CA Cancer J Clin* **74**, 229–263 (2024).
27. Gridelli, C. *et al.* Non-small-cell lung cancer. *Nat Rev Dis Primers* **1**, 15009 (2015).
28. Non-small-cell lung cancer | Nature Reviews Disease Primers. https://www.nature.com/articles/nrdp201548.
29. Brierley, J. *et al.* Global Consultation on Cancer Staging: promoting consistent understanding and use. *Nat Rev Clin Oncol* **16**, 763–771 (2019).
30. Melanoma Skin Cancer Statistics. https://www.cancer.org/cancer/types/melanoma-skin-cancer/about/key-statistics.html.
31. Edmunds, S. C. *et al.* Absence of BRAF gene mutations in uveal melanomas in contrast to cutaneous melanomas. *Br J Cancer* **88**, 1403–1405 (2003).

32. Gordon, R. Skin Cancer: An Overview of Epidemiology and Risk Factors. *Seminars in Oncology Nursing* **29**, 160–169 (2013).
33. European Cancer Information System. https://ecis.jrc.ec.europa.eu/.
34. Saginala, K., Barsouk, A., Aluru, J. S., Rawla, P. & Barsouk, A. Epidemiology of Melanoma. *Med Sci (Basel)* **9**, 63 (2021).
35. Reed, K. B. *et al.* Increasing Incidence of Melanoma Among Young Adults: An Epidemiological Study in Olmsted County, Minnesota. *Mayo Clinic Proceedings* **87**, 328–334 (2012).
36. Sandru, A., Voinea, S., Panaitescu, E. & Blidaru, A. Survival rates of patients with metastatic malignant melanoma. *J Med Life* **7**, 572–576 (2014).
37. Damsky, W. E., Theodosakis, N. & Bosenberg, M. Melanoma metastasis: new concepts and evolving paradigms. *Oncogene* **33**, 2413–2422 (2014).
38. Gershenwald, J. E. *et al.* Melanoma staging: Evidence-based changes in the American Joint Committee on Cancer eighth edition cancer staging manual. *CA: A Cancer Journal for Clinicians* **67**, 472–492 (2017).
39. Puckett, Y., Wilson, A. M., Farci, F. & Thevenin, C. Melanoma Pathology. in *StatPearls* (StatPearls Publishing, Treasure Island (FL), 2024).
40. Treatment. https://www.cancerresearchuk.org/about-cancer/melanoma/treatment.
41. Lipson, E. J. & Drake, C. G. Ipilimumab: An Anti-CTLA-4 Antibody for Metastatic Melanoma. *Clin Cancer Res* **17**, 6958–6962 (2011).
42. Lee, Y. T., Tan, Y. J. & Oon, C. E. Molecular targeted therapy: Treating cancer with specificity. *European Journal of Pharmacology* **834**, 188–196 (2018).
43. Akiteru, G. Molecularly Targeted Therapy: Past, Present and Future. *Chemotherapy: Open Access* **01**, (2012).
44. Nakajima, E. C. *et al.* FDA Approval Summary: Sotorasib for KRAS G12C-Mutated Metastatic NSCLC. *Clin Cancer Res* **28**, 1482–1486 (2022).
45. Jin, H., Wang, L. & Bernards, R. Rational combinations of targeted cancer therapies: background, advances and challenges. *Nat Rev Drug Discov* **22**, 213–234 (2023).
46. Bollag, G. *et al.* Vemurafenib: the first drug approved for BRAF-mutant cancer. *Nat Rev Drug Discov* **11**, 873–886 (2012).
47. Falchook, G. S. *et al.* RAF Inhibitor Dabrafenib (GSK2118436) is Active in Melanoma Brain Metastases, Multiple BRAF Genotypes and Diverse Cancers. *Lancet* **379**, 1893–1901 (2012).
48. Hauschild, A. *et al.* Dabrafenib in *BRAF*-mutated metastatic melanoma: a multicentre, open-label, phase 3 randomised controlled trial. *The Lancet* **380**, 358–365 (2012).

49. Research, C. for D. E. and. FDA approves encorafenib with binimetinib for metastatic non-small cell lung cancer with a BRAF V600E mutation. *FDA* (2023).
50. Research, C. for D. E. and. FDA approves encorafenib and binimetinib in combination for unresectable or metastatic melanoma with BRAF mutations. *FDA* (2018).
51. Flaherty, K. T. *et al.* Improved survival with MEK inhibition in BRAF-mutated melanoma. *N Engl J Med* **367**, 107–114 (2012).
52. Wright, C. J. M. & McCormack, P. L. Trametinib: First Global Approval. *Drugs* **73**, 1245–1254 (2013).
53. Caunt, C. J., Sale, M. J., Smith, P. D. & Cook, S. J. MEK1 and MEK2 inhibitors and cancer therapy: the long and winding road. *Nat Rev Cancer* **15**, 577–592 (2015).
54. Van Allen, E. M. *et al.* The Genetic Landscape of Clinical Resistance to RAF Inhibition in Metastatic Melanoma. *Cancer Discovery* **4**, 94–109 (2014).
55. Long, G. V. *et al.* Dabrafenib plus trametinib versus dabrafenib monotherapy in patients with metastatic *BRAF* V600E/K-mutant melanoma: long-term survival and safety analysis of a phase 3 study. *Annals of Oncology* **28**, 1631–1639 (2017).
56. Planchard, D. *et al.* Dabrafenib plus trametinib in patients with previously untreated BRAFV600E-mutant metastatic non-small-cell lung cancer: an open-label, phase 2 trial. *Lancet Oncol* **18**, 1307–1316 (2017).
57. Planchard, D. *et al.* Phase 2 Study of Dabrafenib Plus Trametinib in Patients With *BRAF* V600E-Mutant Metastatic NSCLC: Updated 5-Year Survival Rates and Genomic Analysis. *Journal of Thoracic Oncology* **17**, 103–115 (2022).
58. Research, C. for D. E. and. FDA grants accelerated approval to dabrafenib in combination with trametinib for unresectable or metastatic solid tumors with BRAF V600E mutation. *FDA* (2022).
59. Holohan, C., Van Schaeybroeck, S., Longley, D. B. & Johnston, P. G. Cancer drug resistance: an evolving paradigm. *Nat Rev Cancer* **13**, 714–726 (2013).
60. Flaherty, K. T. *et al.* Inhibition of mutated, activated BRAF in metastatic melanoma. *N Engl J Med* **363**, 809–819 (2010).
61. Tangella, L. P., Clark, M. E. & Gray, E. S. Resistance mechanisms to targeted therapy in BRAF-mutant melanoma - A mini review. *Biochim Biophys Acta Gen Subj* **1865**, 129736 (2021).
62. Catalanotti, F. *et al.* PTEN Loss-of-Function Alterations Are Associated With Intrinsic Resistance to BRAF Inhibitors in Metastatic Melanoma. *JCO Precision Oncology* (2017) doi:10.1200/PO.16.00054.
63. Cabanos, H. F. & Hata, A. N. Emerging Insights into Targeted Therapy-Tolerant Persister Cells in Cancer. *Cancers* **13**, 2666 (2021).

64. Sun, C. *et al.* Reversible and adaptive resistance to BRAF(V600E) inhibition in melanoma. *Nature* **508**, 118–122 (2014).
65. Shen, S., Vagner, S. & Robert, C. Persistent Cancer Cells: The Deadly Survivors. *Cell* **183**, 860–874 (2020).
66. Bigger, JosephW. Treatment of Staphylococcal Infections with Penicillin by Intermittent Sterilisation. *The Lancet* **244**, 497–500 (1944).
67. Balaban, N. Q. *et al.* Definitions and guidelines for research on antibiotic persistence. *Nat Rev Microbiol* **17**, 441–448 (2019).
68. Hata, A. N. *et al.* Tumor cells can follow distinct evolutionary paths to become resistant to epidermal growth factor receptor inhibition. *Nat Med* **22**, 262–269 (2016).
69. Vallette, F. M. *et al.* Dormant, quiescent, tolerant and persister cells: Four synonyms for the same target in cancer. *Biochemical Pharmacology* **162**, 169–176 (2019).
70. Ramirez, M. *et al.* Diverse drug-resistance mechanisms can emerge from drug-tolerant cancer persister cells. *Nat Commun* **7**, 10690 (2016).
71. Shaffer, S. M. *et al.* Rare cell variability and drug-induced reprogramming as a mode of cancer drug resistance. *Nature* **546**, 431–435 (2017).
72. Boumahdi, S. & de Sauvage, F. J. The great escape: tumour cell plasticity in resistance to targeted therapy. *Nat Rev Drug Discov* **19**, 39–56 (2020).
73. Vinogradova, M. *et al.* An inhibitor of KDM5 demethylases reduces survival of drug-tolerant cancer cells. *Nat Chem Biol* **12**, 531–538 (2016).
74. Warburg, O., Wind, F. & Negelein, E. The metabolism of tumors in the body. *Journal of General Physiology* **8**, 519–530 (1927).
75. Kierans, S. J. & Taylor, C. T. Regulation of glycolysis by the hypoxia-inducible factor (HIF): implications for cellular physiology. *J Physiol* **599**, 23–37 (2021).
76. Kluza, J. *et al.* Inactivation of the HIF-1α/PDK3 signaling axis drives melanoma toward mitochondrial oxidative metabolism and potentiates the therapeutic activity of pro-oxidants. *Cancer Research* **72**, 5035–5047 (2012).
77. Corazao-Rozas, P. *et al.* Mitochondrial oxidative phosphorylation controls cancer cell's life and death decisions upon exposure to MAPK inhibitors. *Oncotarget* **7**, 39473–39485 (2016).
78. Roesch, A. *et al.* Overcoming Intrinsic Multidrug Resistance in Melanoma by Blocking the Mitochondrial Respiratory Chain of Slow-Cycling JARID1Bhigh Cells. *Cancer Cell* **23**, 811–825 (2013).
79. Zhu, J. & Thompson, C. B. Metabolic regulation of cell growth and proliferation. *Nat Rev Mol Cell Biol* **20**, 436–450 (2019).

80. Shen, S. *et al.* Melanoma Persister Cells Are Tolerant to BRAF/MEK Inhibitors via ACOX1-Mediated Fatty Acid Oxidation. *Cell Rep* **33**, 108421 (2020).
81. Kumari, A. Beta Oxidation of Fatty Acids. in *Sweet Biochemistry* 17–19 (Elsevier, 2018). doi:10.1016/B978-0-12-814453-4.00004-2.
82. Aloia, A. *et al.* A Fatty Acid Oxidation-dependent Metabolic Shift Regulates the Adaptation of *BRAF* -mutated Melanoma to MAPK Inhibitors. *Clinical Cancer Research* **25**, 6852–6867 (2019).
83. Theodosakis, N. *et al.* BRAF Inhibition Decreases Cellular Glucose Uptake in Melanoma in Association with Reduction in Cell Volume. *Molecular Cancer Therapeutics* **14**, 1680–1692 (2015).
84. Hernandez-Davies, J. E. *et al.* Vemurafenib resistance reprograms melanoma cells towards glutamine dependence. *J Transl Med* **13**, 210 (2015).
85. Smith, L. K. *et al.* Adaptive translational reprogramming of metabolism limits the response to targeted therapy in BRAFV600 melanoma. *Nat Commun* **13**, 1100 (2022).
86. Sharma, S. V. *et al.* A chromatin-mediated reversible drug-tolerant state in cancer cell subpopulations. *Cell* **141**, 69–80 (2010).
87. Long, G. V. *et al.* Adjuvant Dabrafenib plus Trametinib in Stage III BRAF-Mutated Melanoma. *N Engl J Med* **377**, 1813–1823 (2017).
88. Huang, C., Radi, R. H. & Arbiser, J. L. Mitochondrial Metabolism in Melanoma. *Cells* **10**, 3197 (2021).
89. Riss, T. L. *et al.* Cell Viability Assays. in *Assay Guidance Manual* (eds. Markossian, S. et al.) (Eli Lilly & Company and the National Center for Advancing Translational Sciences, Bethesda (MD), 2004).
90. Haq, R. *et al.* Oncogenic BRAF regulates oxidative metabolism via PGC1α and MITF. *Cancer Cell* **23**, 302–315 (2013).
91. Zhang, G. *et al.* Targeting mitochondrial biogenesis to overcome drug resistance to MAPK inhibitors. *Journal of Clinical Investigation* **126**, 1834–1856 (2016).
92. Shen, S. *et al.* An epitranscriptomic mechanism underlies selective mRNA translation remodelling in melanoma persister cells. *Nat Commun* **10**, 5713 (2019).
93. Karki, P., Angardi, V., Mier, J. C. & Orman, M. A. A Transient Metabolic State in Melanoma Persister Cells Mediated by Chemotherapeutic Treatments. *Front. Mol. Biosci.* **8**, 780192 (2022).
94. Hong, S.-K., Starenki, D., Wu, P.-K. & Park, J.-I. Suppression of B-Raf ^{V600E} melanoma cell survival by targeting mitochondria using triphenyl-phosphonium-conjugated nitroxide or ubiquinone. *Cancer Biology & Therapy* **18**, 106–114 (2017).